(2)

NAVAL POSTGRADUATE SCHOOL
Monterey, California

THESIS

AN EXAMINATION OF DELTA PRIME GROWTH IN AN ALUMINUM-LITHIUM ALLOY BY X-RAY DIFFRACTION

by

Clark E. Whitman

March 1990

Thesis Advisor A.G. Fox

Unclassified

security classification of this page

REPORT DOCUMENTATION PAGE

1a Report Security Classification Unclassified			1b Restrictive Markings
2a Security Classification Authority			3 Distribution/Availability of Report
2b Declassification Downgrading Schedule			Approved for public release; distribution is unlimited.
4 Performing Organization Report Number(s)			5 Monitoring Organization Report Number(s)
6a Name of Performing Organization Naval Postgraduate School	6b Office Symbol *(if applicable)* 34		7a Name of Monitoring Organization Naval Postgraduate School
6c Address *(city, state, and ZIP code)* Monterey, CA 93943-5000			7b Address *(city, state, and ZIP code)* Monterey, CA 93943-5000
8a Name of Funding Sponsoring Organization	8b Office Symbol *(if applicable)*		9 Procurement Instrument Identification Number
8c Address *(city, state, and ZIP code)*			10 Source of Funding Numbers
			Program Element No / Project No / Task No / Work Unit Accession No

11 Title *(include security classification)*
AN EXAMINATION OF DELTA PRIME GROWTH IN AN ALUMINUM-LITHIUM ALLOY BY X-RAY DIFFRACTION

12 Personal Author(s) Clark E. Whitman

13a Type of Report	13b Time Covered	14 Date of Report *(year, month, day)*	15 Page Count
Master's Thesis	From To	March 1990	58

16 Supplementary Notation The views expressed in this thesis are those of the author and do not reflect the official policy or position of the Department of Defense or the U.S. Government.

17 Cosati Codes			18 Subject Terms *(continue on reverse if necessary and identify by block number)*
Field	Group	Subgroup	Aluminum-Lithium Alloys, Microstructural development

19 Abstract *(continue on reverse if necessary and identify by block number)*

A previously manufactured hot rolled sheet of Al-Li-Zr alloy of composition Al-2.5%Li-.15%Zr, by weight, was solution treated and artificially aged at 194°C from 0 to 32 hours. X-ray diffraction analysis of the alloy was conducted to observe the growth characteristics of the delta prime precipitate (the precipitate hardening phase). Transmission electron microscopy was used to verify X-ray results. Significant superlattice intensity and line broadening occurred in the as-quenched sample. This observation supports a possible order/disorder reaction and a spinodal decomposition as opposed to the typical nucleation and precipitation reaction usually observed in a precipitation hardened alloy. The Scherrer equation was used to determine delta prime particle size from diffraction line broadening, and this size was found to coarsen following conventional Ostwald ripening theory once the initial effects of the spinodal had aged out. The delta phase (considered cause of low toughness) was observed in the as quenched sample and throughout the heat treatment. It was surmised that this may be the origin of the low short-transverse fracture toughness which is typical of some of these alloys. Theses. (JS)

20 Distribution Availability of Abstract	21 Abstract Security Classification	
☒ unclassified unlimited ☐ same as report ☐ DTIC users	Unclassified	
22a Name of Responsible Individual A.G. Fox	22b Telephone *(include Area code)* (408) 663-3275	22c Office Symbol 54Ss

DD FORM 1473,84 MAR — 83 APR edition may be used until exhausted / All other editions are obsolete — security classification of this page

Unclassified

Approved for public release; distribution is unlimited.

An Examination of Delta Prime Growth in an Aluminum-Lithium Alloy By X-Ray Diffraction

by

Clark E. Whitman
Lieutenant , United States Navy
B.S., Wright State University, 1979

Submitted in partial fulfillment of the
requirements for the degree of

MASTER OF SCIENCE IN MECHANICAL ENGINEERING

from the

NAVAL POSTGRADUATE SCHOOL
March 1990

Author: Clark E. Whitman

Clark E. Whitman

Approved by: Alan G. Fox

A.G. Fox, Thesis Advisor

Anthony J. Healey, Chairman,
Department of Mechanical Engineering

ABSTRACT

A previously manufactured hot rolled sheet of Al-Li-Zr alloy of composition Al-2.5%Li-.15%Zr, by weight, was solution treated and artificially aged at 194°C from 0 to 32 hours. X-ray diffraction analysis of the alloy was conducted to observe the growth characteristics of the delta prime precipitate (the precipitate hardening phase). Transmission electron microscopy was used to verify X-ray results. Significant superlattice intensity and line broadening occurred in the as-quenched sample. This observation supports a possible order/disorder reaction and a spinodal decomposition as opposed to the typical nucleation and precipitation reaction usually observed in a precipitation hardened alloy. The Scherrer equation was used to determine delta prime particle size from diffraction line broadening, and this size was found to coarsen following conventional Ostwald ripening theory once the initial effects of the spinodal had aged out. The delta phase (considered cause of low toughness) was observed in the as quenched sample and throughout the heat treatment. It was surmised that this may be the origin of the low short-transverse fracture toughness which is typical of some of these alloys.

TABLE OF CONTENTS

LIST OF TABLES

LIST OF FIGURES

I. INTRODUCTION

The benefits and advantages of aluminum have been widely known and exploited through the years. In the aeronautics industry few, if any, other alloys or materials have been able to succesfully show superiority to its efficient combination of strength, weight and cost. Yet, the search for lighter, stronger materials to engineer faster, higher payload, more fuel efficient aircraft or aerospace vehicles has spurred the development of advanced materials. These materials, namely composites, have challenged the aluminum industry to create even more effective aluminum alloys.

The new formulations to meet the "composite challenge" are the aluminum-lithium alloys. Each addition of one weight percent lithium decreases the density by 3% while increasing the elastic modulus by 6%. This can continue up to approximately 4%. Optimally, this would create a material that is 12% lighter yet 24% stiffer than current aircraft grade aluminum alloys.

This optimum lithium addition has yet to be achieved without creating other damaging side effects (e.g. low toughness). Additions of up to 2.6% though, are now commercially available as direct substitutes for alloys 7075 and 2024, the current aircraft alloys. Continued metallurgical research is exploring various alloying additions and heat/rolling treatments to maximize the Al-Li low density, high stiffness potential.

Yet, even though the alloy is available commercially, there are still basic questions being asked about the microstructural development of the alloy. The Al_3Li particle, called delta prime (δ') is considered the main strenthening or precipitation hardening element in the alloy. The formation and development of the δ' is not completely understood. It is anticipated that through basic research the low toughness problem, still occurring, can be resolved. The production of more pure Al-Li alloys (i.e. less non-Lithium alloying additions) is also desired.

Although much work has been done using the Transmission Electron Microscope (TEM), this study will primarily use X-Ray diffraction analysis. By use of the Scherrer equations, the particle size of the δ' will be determined for a sample from quench to peak strength heat treatment. Due to limits on the resolution capabilities of the NPS Transmission Electron Microscope(TEM), an as-quenched sample cannot be directly compared to the X-Ray results but a peak aged sample will be used to verify the accuracy of the technique.

II. BACKGROUND

A. ALLOY HISTORICAL DEVELOPMENT

With the development of heat treatable aluminum alloys, such as Duralumin, prior to World War I, industrial efforts were aimed at producing stronger, lighter, more easily fabricated, more corrosion resistant aluminum alloys. Lithium additions were naturally considered very early on due to lithium being one of only eight elements whose solid solubilities in aluminum exceeds one atomic percent. (only three other elements have higher solid solubilities). Although patent filings occurred as early as 1919 in Germany (Scleron), the exact effects of the early lithium additions were not clear and the additions may have been motivated more by patent rights rather than material improvements. [Ref.1].

Continued research, development, and production of aluminum- lithium was always overshadowed by improvements and subsequent demand for the Al-Cu-Mg type alloys. Yet, in 1958, a major milestone occurred with the Aluminum Company of America's (ALCOA) production of alloy 2020 (Al-4.5Cu-1.1Li-.5Mn-.2Cd). This alloy benefitted from lower density, increased elastic modulus (i.e., stiffer), and increased resistance to exfoilation corrosion and stress corrossion cracking. The main drawback was that the new alloy had a lower toughness than the current comparable aircraft alloy (e.g., 7075). 2020 was put into service though, by North American Aviation (now Rockwell Intl.) on the U.S. Navy RA-5C Vigilante aircraft already in production. 177 aircraft were built with the upper and lower skins of the wing and horizontal stabilizers manufactured from 2020. Design considerations included the greater "notch sensitivity" of the new alloy. Total weight saved was 73 kg. The application was (and still is) considered a success. Low toughness, though, still remained a major concern. Lack of demand for the alloy resulted in the shutdown of the ALCOA production facilities in 1969. [Ref.1].

Meanwhile, research in the USSR resulted in the development of alloy 01420(Al-5.Mg-2.Li-.5Mn) which was patented in France and Britian in 1968 and 1969, respectively. This alloy was eventually used in the MiG-25 Foxbat [Ref.2]. In Great Britan, extensive work was being conducted at Fullmer Research for the Royal Air Force.

Through the 1970's and 1980's continued research and development was accelerated due to such factors as:

- Desire for weight savings and fuel economy.
- Greater aircraft speeds and mobility.
- Advent of other competetive materials.
- Concern about USSR aircraft superiority.
- Continued alloying and production successes. [Ref.2]

The main driving force for development has obviously been due to the aircraft and aerospace industries (for commercial and military applications). *Any* lighter, stronger material is desired. Lower vehicle weight means faster speed, or greater payload, or less fuel consumption. Yet, the attraction to a new aluminum alloy is even more alluring.

Specific benefits, when compared to other exotic materials (namely composites) are:

- *Tooling.* Machinery and skills to form are already available.
- *Engineering.* Aluminum engineering database already established. Simple repair procedures tested and proven. Aluminum-lithium's overall engineering response is considered very balanced. Although not the strongest nor the lightest , it does not contain any major drawbacks or weak points. [Ref.3].
- *Production.* Design changes considered easy to implement during production runs.
- *Safety.* Crash performance preferrable to wood-like splintering of composites. (This is very relevant considering the two commercial airline crashes that have occurred in the past year in which the majority of the passengers have survived.) [Ref.4].
- *Superplasticity.* Aluminum-lithium is also capable of being formed into intricate continuous piece shapes. Elongations of up to one thousand percent have been reported. [Ref.5].

The drawbacks have been:

- *Low Toughness.* This once major problem has basically been overcome in the new 2090 and 8090 series alloys except for the short-transverse direction. [Ref.6].
- *Cost.* The reactivity of lithium with moisture, corrosion products and air has been a continual problem during production. Effective production methods have been developed albeit at a price. Aluminum-lithium alloys are currently *2-4 times the cost of the conventional alloys* to produce.

Other concerns have been:

- *Scrap Segregation.* Effective recycling can only occur if the lithium containing aluminum remains separate. Industry considers this a minor problem. [Ref.7].
- *Lithium Availability.* A possible lithium shortage was predicted in a 1977 study. a 1985 re-evaluation did not predict any supply problems. [Ref.8]

B. CURRENT STATUS

The "state of the art" in commercially available aluminum-lithium alloys are the first four composition entries in Table 1 below. The last two entries are the current non-lithium aerospace alloys being used today.

Table 1. CONVENTIONAL AND ALUMINUM-LITHIUM ALLOY COMPOSITIONS (Nominal Weight %) [Ref.2].

alloy	Li	Cu	Mg	Mn	Zr	Zn	Cr
2090	2.2	2.8	--	--	0.1	--	--
8091	2.6	2.0	0.9	--	0.1	--	--
2091	2.0	2.2	1.5	--	0.1	--	--
8090	2.5	1.3	1.0	--	0.1	--	--
2024	--	4.4	1.5	0.6	--	--	--
7075	--	1.6	2.5	--	--	5.6	0.2

Current intended commercial applications include the Airbus Industrie (France) A320, A310, and A300-600, and the Boeing company new 7J7 airplane as well as a broader application, by Boeing, throughout their entire product line. [Refs.7,4].

The US Air Force has been testing an F15D wing skin machined from 8090. A weight savings of 24 pounds was realized, the panel performance was increased, and the fatigue life (using an F15E, 9g flight spectrum) was increased from 18,000 to 40,000 hours. The first test flight was in 1986. [Ref.9].

The US Navy has been sponsoring a development program through the Naval Air Development Center and ALCOA to concentrate on the following goals:

- 7075-T6 replacement with 2090-T8E41.(Maximum strength material)
- 7075-T73 replacement with 2090 or 8092.(Stress corrossion resistant materials)

Thirty government and private laboratories have been conducting testing on alloys supplied by ALCOA. Table 2 on page 5 and Table 3 on page 5 were obtained from that analysis. [Ref.10].

Table 2. 2090 VS. 7075 TEST DATA [Ref.10]

	UTS KSI	TYS KSI	Elong. %	E(T) MSI	E(C) MSI
2090(L)	85	75	7.6	11.5	12.0
7075(L)	83	78	12.	10.3	10.6
2090(LT)	85	80	6.2	11.6	12.1
7075(LT)	84	75	12.	10.3	10.6

Table 3. 2090 VS. 7075 FRACTURE TOUGHNESS [Ref.10]

Alloy	Fracture Toughness $K_Q(Ksi-in^{1/2})$
2090 (L-T)	29
7075 (L-T)	26
2090 (T-L)	28
7075 (T-L)	23

Exposure panels have been installed on selected ships and a one foot square access panel has also been installed on fleet F-18s for in-service testing. Additional research is to be conducted on the superplascticity capabilities. Current concerns are the low toughness being experienced in the short-transverse direction and the lack of consistent engineering property anistropy in commercial plate greater than one half inch thick. [Ref.6].

C. MICROSTRUCTURE

Although current commercial applications use quaternary and greater alloys, this study will be limited to the Al-Li-Zr system.

1. Methods of Analysis

Characterization of this alloy system, and thus its phase diagram, is hampered by analysis difficulties. The precipitates usually examined in Al-Li alloys are the δ' , δ (Al-Li), Al_3Zr, and possibly others depending on alloying additions. The small size of the δ' particles and the presence of Li are the two major obstacles to analysis. Sung recommended using instruments with less than a 500Å spatial resolution and less than a 3% Li(weight) capability for quantitative analysis. [Ref.11].

The following quantitative methods are summarized:

- *X-Ray Microanalysis* is not possible because the energy of Li-K_α X-Rays cannot be detected with windowless or crystal spectrometers. [Ref.12].
- *Ionization EELS.* Minimum Li detectability is about 3% but spatial resolution is less than 500Å.[Refs.11,12].
- *Plasmon EELS.* Minimum detectability is less than 1% and the spatial resolution is less than 100Å. This equipment, though, is not very common and data generation analysis is very time consuming. [Ref.11].
- *Convergent Beam Electron Diffraction (CBED).* Sung et al noted a change in lattice parameter of δ' with aging, which implies a composition change, but the data could not be easily interpreted. [Ref.11].
- *Atom Probe Field Ion Microscopy.* This technique can analyze all elements with equal efficiency. Spatial resolution and quantitative capabilities determined from recent studies are sufficient for Al-Li alloy research [Ref.13].

Particle size determination, specifically of δ', has been accomplished by Transmission Electron Microscopy (TEM). Spooner reported that TEM, though, is severely limited by its statistical sampling due to the small volume of sample size. The sampling is critical to calculations involving precipitation kinetics, growth or coarsening, volume fractions or particle size distributions. In their study, combined Small Angle X-Ray Scattering (SAXS) proved to be advantageous to TEM, in many ways. [Ref.14].

X-Ray diffraction analysis can also be used for size determination and volume fraction as demonstrated by this thesis.

2. Phase Diagram

The strength of this alloy is due to the presence of the δ' (delta prime) precipate. As can be seen in the Al-Li phase diagram Figure 1, which is still being investigated, a 460° solution heat treatment of a 2.5%(wt.) Li alloy (as per this study) will produce the disordered α phase, a face centered cubic of Al and Li.

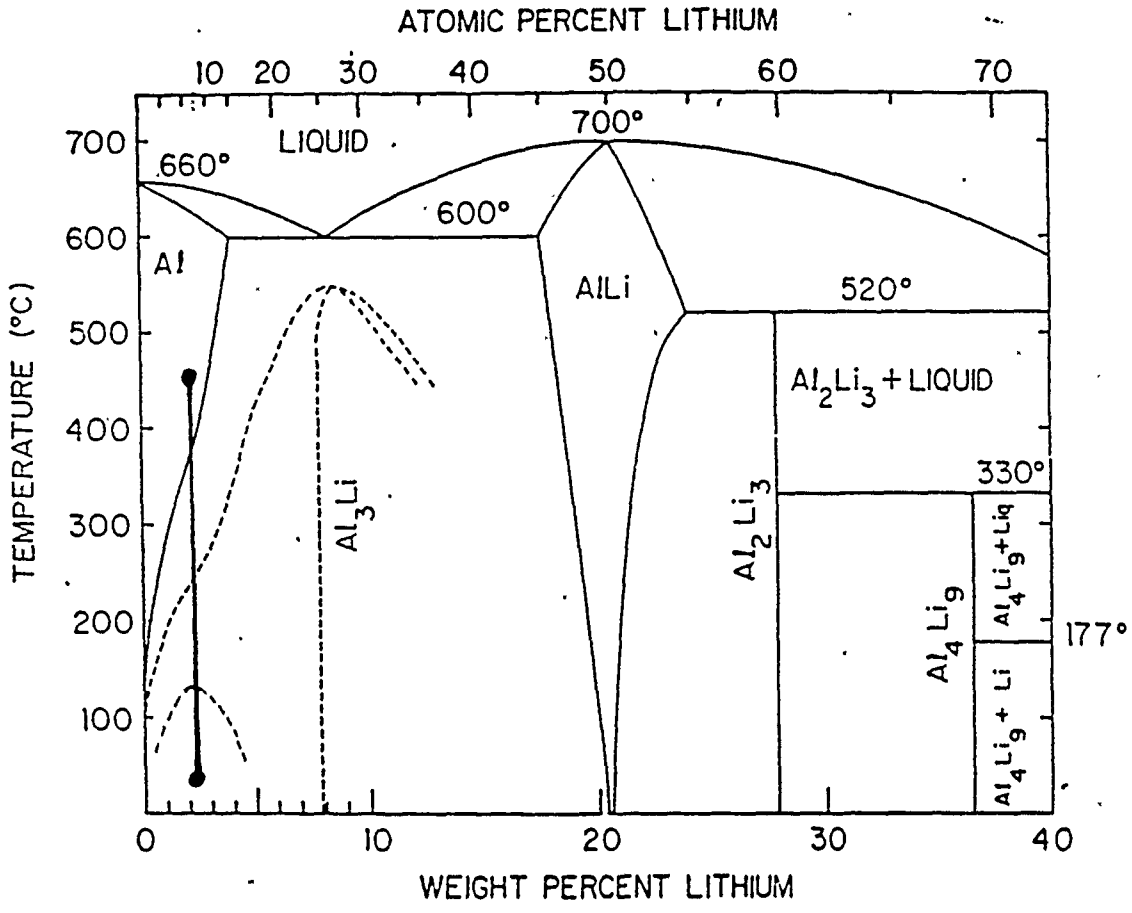

Figure 1. Al-Li Phase Diagram: Vertical bar indicates quench. Upper dashed line is proposed order/disorder region. Bottom dashed line is proposed miscibility gap.[Ref.15].

Immediately upon quenching into the proposed miscibility gap, δ' forms in the α matrix. δ' is a face centered cubic approximating a composition ratio of 3Al:1Li when fully ordered. The δ' growth in the α matrix acts as a precipitation hardener. A close-up of the miscibility gap region of the phase diagram is shown in Figure 2 [Ref.11].

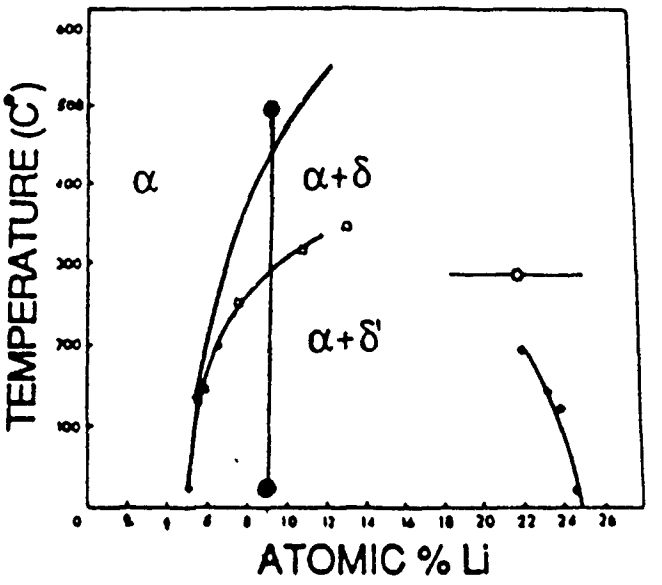

Figure 2. Miscibility Gap region of Phase Diagram

3. Phase Descriptions

a. $\delta'(Al_3Li)$

δ' is a face centered cubic, L12 structure (Figure 3), with a unit cell dimension of 4.045Å. This structure is also referred to as a superlattice. The particle itself forms spherically and initially remains coherent within the matrix (misfit less than .2%). The longer the aging time, or the lower the Li%(of alloy), the more spherical the particle. Coarsening is accelerated by increasing the Li content, the aging temperature, or by the addition of zirconium. [Ref. 16] At longer aging times or higher aging temperatures coherency is eventually lost.[Ref.17].

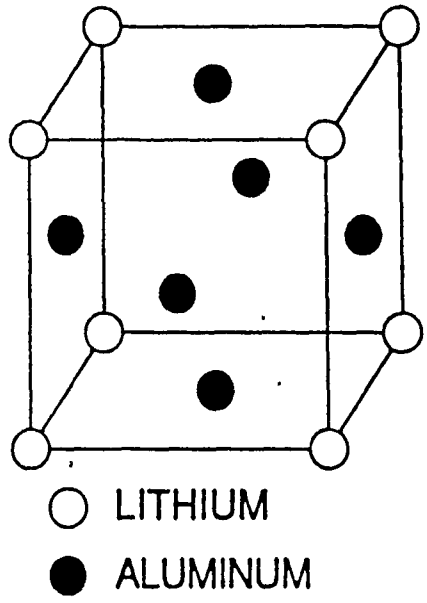

Figure 3. L12 Ordered Structure of $\delta'(Al_3Li)$

The composition of δ' is usually not a stoichiometric ratio. The Li content increases with aging time until the limits of the proposed miscibility gap value is attained [Ref.18].

The particle size distribution (PSD) can be modeled by a Weibull distribution. The skewness (i.e. extended right or left tail) of the distribution is dependent upon alloy Li percentage. Symmetrical shape being attained at Li≈3.8% for binary alloys. Zr additions will cause skewness towards larger particle sizes. [Ref.19].

The growth follows Ostwald ripening kinetics: $\overline{R}^3 = K \times t$, where $\overline{R}$ equals average particle size, K equals a constant, and t equals time. Gu et al compared the growth to various Ostwald ripening theories. The Lifshitz-Slyozov Encounter Modified(LSEM) theory was the most accurate in modeling the PSD. Yet, the LSEM assumes that any two closely spaced particles will coalesce. They did not observe the existence of any anti-phase boundaries in the δ' particles and thus concluded that only those particles in crystallgraphic registry will coalesce. Their general conclusion was that to accurately model the coarsening process, especially at high volume fractions, the coalescence mechanism must be considered. [Refs.16,20].

b. Al_3Zr)

The effect of Zirconium additions to Al-Li alloys is to retard recrystallization, control grain growth, and to improve toughness, stress corrosion, and quench sensitivity [Ref.17]. This is accomplished by the Al_3Zr phase. Al_3Zr is also a face centered cubic, L12 structure with a unit cell dimension of 4.08Å [Ref.21]. It has a slight positive misfit with the α matrix. The δ' has a slight negative misfit thus the Al_3Zr serves as a nucleation or "wetting" site for the δ'. Al_3Zr does not solutionize at Al-Li solutionizing temperatures, and is immediately present during the quench as 200-300Å spheres.[Ref.22].

Pickering et.al.,conducted composition studies on Al_3Zr using Field Ion Microscopy(FIM) and Atom Probe Field Ion Microscopy(APFIM). The Al_3Zr contained approximately 5-11%at. Li in the as quenched sample which declined to 1-7% with aging. They concluded that very little Li is incorporated, and that the Al_3Zr composition can be considered almost stoichiometric. [Ref.13].

c. δ(Al-Li)

δ is considered an equilibrium intermetallic, body centered cubic of B32(NaTl) structure. The unit cell dimension is 6.37Å. δ is considered more stable than δ'. [Ref.23].

δ has been observed to preferentially form along high angle grain boundaries and also within the matrix at longer aging times [Ref.24]. No evidence could be found in current literature for the presence of δ in the as quenched state. δ has been seen after .25 hour in TEM micrographs [Ref.24]. It has been noted that electropolishing techniques can react with the δ and thus remove it from the sample section [Ref.23].

The formation of δ has been suggested (Niskanen et.al) to occur via the preferential coarsening of δ'[Ref.25] , i.e.:

$$\alpha \rightarrow \delta' \rightarrow \delta$$

It has also been proposed (Williams) that the δ nucleates heterogeneously on the grain boundary and within the matrix independently of δ' [Ref.26], i.e.:

$$\alpha \rightarrow \delta$$

The growth of the δ occurs through the dissolution of the δ' particles. This is evidenced by a Precipitate Free Zone (PFZ) which forms at the grain boundaries and also surrounds the matrix δ particles. [Ref.24].

4. $\delta'(Al_3Li)$ Precipitation Theory

Generally, all TEM studies conducted have noted the existence of superlattice reflections in the as-quenched alloy. Recently (1989), X-Ray studies by Fox et al [Ref.27] have also produced these same superlattice reflections. The reflections indicate the presence of δ' or of ordered regions. To date, no researchers have been able to suppress the δ' formation during the quench in alloys over 5.5 %at.Li.

The δ' formation process has been considered as a coherent nucleation and growth or as a spinodal decomposition. In 1975, Williams and Edgington reported that if a spinodal decomposition were occurring, the expected periodic distribution of particles should give X-Ray sideband structures and satellites on diffraction patterns. These were not seen, but the predicted sideband intensity is only 1/600 of the fundamental peak intensity. Thus, evidence has not come forth to disprove a spinodal decomposition.[Ref.28].

Others, such as Spooner, Williams and Sung, have given evidence for a spinodal decomposition path. Using SAXS data, a rise and fall in the particle radius (termed the Guinier radius) was observed. They interpreted this anomaly as a spinodal decomposition in the matrix with fast coarsening, and then the nucleation of more stable δ' of a smaller size.[Ref.14].

A recent (1986) theoretical model was presented by Khachaturyan and is shown in Figure 4 [Ref.29].

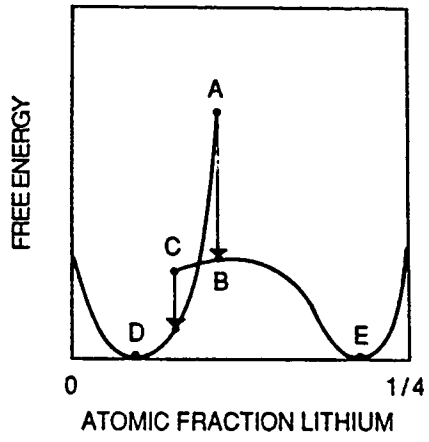

Figure 4. Order/Disorder and Spinodal Decomposition Model

Following from A to D and E during the quench:

A	Disordered solid solution of composition A
A→B	Solution orders congruently(i.e. overall composition retained) to B, but B is unstable with respect to spinodal decomposition.
B→C	B spinodally decomposes to C, but Li lean ordered product is unstable with respect to disorder.
C→D	C disorders to D, i.e. the disordered matrix.
B→E	B spinodally decomposes to E. E remains ordered and Li rich, i.e. the δ' particles.

Sato et al have imaged the ordered regions using High Resolution Electron Microscopy (HREM). These regions were easily distinguished from the disordered matrix, but not so easily from the δ' which also immediately forms. [Ref.30]. Similar HREM micrographs have been produced by Fox (See Figure 8 on page 25). This evidence supports the spinodal decomposition model.

5. Phase Effects on Engineering Properties

a. Modulus of Elasticity

The increased stiffness of Al-Li alloys was originally thought to have been due to the δ' precipitates. Studies by Noble et.al, though, have shown that the modulus of elasticity is higher in the as quenched state as compared to pure aluminum. Additional ageing provides only small increases in stiffness. Fox and Fisher proposed an electronic theory to explain this observation. They theorized that since the nearest neighbor (n-n) distance in the pure Li is 3.031Å whereas this same n-n distance in Al-Li solid solution is 2.86Å, the valence electrons are compacted into a much smaller volume. The resultant increase in n-n atom force constants translates into a higher Debye temperature, and thus a higher modulus of elasticity with increasing Li content. This theory explains both the as quenched modulus and the increase of the modulus with aging. [Refs.31,32].

b. Strength and Toughness

In the underaged or nearly aged to peak strength Al-Li alloy, the dislocations move in pairs. The first dislocation cuts through the δ', destroys the order, thus creating antiphase boundaries (APB) in the particles. The second dislocation restores the order removed by the first. For a very fine dispersion, the dislocations are almost straight. As the δ' particles grow, the dislocations become waivier. In the peak aged state (at a critical radius) the dislocations are entirely in the matrix curving around the precipitates. The δ' is not being sheared. The separation distance of the dislocations is one or two times the particle size. With continued aging, and particle size growth, the dislocations bypass the particles. Dislocation loops (i.e., Orowan) are left around the particles, and alloy strength declines.[Ref.33]. The critical size just prior to looping is 300Å [Refs.34,19] to 500Å [Ref.35].

Noble et.al, have proposed that the strength at peak age is mainly due to order hardening (the creation of APBs in the δ'), or by a combination of order hardening and modulus hardening(difference between modulus of precipitate and matrix).[Ref.36]. Furukawa et al also concur that APB resistance to the dislocation movement is a major strengthener, but they also believe that the friction stresses due to δ' and the matrix are the additional dominant contributors. [Ref.33].

Noble et. al., have concluded that although δ' shearing provides high strength, it also causes intense planar slip. Stress concentrations are created where the slip bands meet the grain boundaries and the result is brittle intergranular failure. They also noted that the presence of δ(Al-Li) is undesireable. [Ref.36].

Sanders et .al., reported that at shorter aging times, when grain boundary precipitates and PFZs are absent, fracture occurs transgranularly. At longer aging times ductile fracture occurs intergranularly along the PFZ.[Ref.37].

Furukawa et al noted that in high Li (> 11.1%at.) alloys, planar slip was not seen and other mechanisms must account for the low ductility [Ref.35].

D. BASIS OF X-RAY DIFFRACTION STUDIES

1. Particle Size

X-Ray diffraction can be used to determine particle (i.e., δ') size by analysis of the diffraction profiles. Diffraction theory predicts that a polycrystalline specimen consisting of large strain-free crystals will produce sharp (breadths measured in seconds of arc) diffraction lines. In practice this never happens. Mean precipitate size, lattice strain, and instrumental error can all contribute to line broadening.

Although there are complicated methods for analyzing the diffraction profile such as Fourier-Transform or Iterative Folding, there are also simplified methods which depend on direct measurements of the profile width. The profile width can either be measured directly at half maximum, or the integral breadth (area divided by height) can be used. If the line shape is assumed to be Gaussian, the following relationship would be used to determine the pure diffraction profile (which contains the particle size information):

$$B^2 = b^2 + \beta^2$$

B	Experimental width (half maximum or integral) measured directly from instrument output.
b	Instrumental and physical factors(strain). Instrumental broadening is determined by analyzing a standard (e.g. quartz) that should produce no broadening. Physical broadening is considered zero for this application.
β	Pure profile. This remaining profile width will contain particle size information.

Upon obtaining β, the particle size can be obtained from the Scherrer equation:

$$L = \frac{K\lambda}{\beta \cos\theta}$$

L	Particle size (diameter) in Å.
K	A constant ≈ 1.
θ	θ value from Bragg equation.
β	Pure diffraction profile expressed in radians.
λ	X-Ray wavelength in Å.

For size determination of a strain-free sample, the optimum experimental conditions are those minimizing **b** and maximizing **B**. Up to approximately 300-400 Å, all analysis methods prove equally effective. But, in the 400 to 2000Å range, greater refinements to the calculations are required. Over approximately 2000Å(1000Å for Debye-Scherrer cameras, 3000Å for high resolution diffractometers) line broadening due to particle size is effectively absent. [Ref.38].

2. Volume Fraction

By comparing the intensities (number of counts under the diffraction profile) generated by the fundamental and superlattice diffraction peaks, it is possible to calculate the volume fraction of the superlattice precipate. In this study the 100 superlattice of the δ' is compared to the 200 fundamental of the matrix and δ'.

The X-Ray structure factors must first be developed. The structure factor F is defined as the ratio of the amplitude scattered by the plane (hkl) relative to the amplitude scattered by a single electron. Consider a B rich B_3A L12 alloy (such as δ'). A atoms occupy a sites, and B atoms occupy b sites in the fully ordered or stoichiometric alloy. If not fully ordered the atoms and sites may be interchanged. This situation is covered by the following (partial) structure factors [Ref.39]:

$$F_F^{\alpha,\delta'} = \bar{f}[3\exp(-M_b) + \exp(-M_a)] + .75\Delta f S \times [\exp(-M_b) - \exp(-M_a)] \quad (1)$$

$$F_S^{\delta'} = \bar{f}[\exp(-M_b) - \exp(-M_a)] + .25\Delta f S \times [3\exp(-M_a) + \exp(-M_b)] \quad (2)$$

$F_F^{\alpha \text{ or } \delta'} = fundamental\ from\ \alpha \text{ or } \delta'$ $\quad f_{B \text{ or } A} = free\ atom\ form\ factors$

$F_S^{\delta'} = superlattice\ from\ \delta'$ $\quad \bar{f} = m_A f_A + m_A f_B$

$M_{a \text{ or } b} = temperature\ factor$ $\quad m_{A \text{ or } B} = atomic\ fraction\ of\ A\ or\ B$

$S = long\ range\ order$ $\quad \Delta f = f_B - f_A$

$S\ must\ satisfy\ 0 \le S \le S_{max}$ $\quad S_{max} = (4/3)m_B\ for\ m_A \ge .25$

$S_{max} = 4m_A\ for\ m_A \le .25$

For a B rich alloy, assuming $M_a = M_b = M$, equations (1) and (2) become:

$$F_F^{\alpha \text{ or } \delta'} = 4(m_A^{\alpha \text{ or } \delta'} f_A + m_B^{\alpha \text{ or } \delta'} f_B) \exp(-M) \tag{3}$$

$$F_S^{\delta'} = S_{\max}(f_B - f_A) \exp(-M) \tag{4}$$

Where $S_{\max} = 4\, m_A$, and noting that exp(-M) can be ignored (i.e. equal to 1) if the ratio of the equations is used. The overall structure factors are:

$$F_S^2 = V_f(F_S^{\delta'})^2 \tag{5}$$

$$F_F^2 = (1 - V_f)(F_F^{\alpha})^2 + V_f(F_F^{\delta'})^2 = (F_F^{\alpha})^2 - V_f(F_F^{\alpha})^2 + V_f(F_F^{\delta'})^2 \tag{6}$$

Where V_f= volume fraction (an unknown), and equations (3) and (4) are inserted appropriately. Now considering the 100 and 200 peaks:

$$\frac{I_{100}}{I_{200}} = \frac{\phi^{100}}{\phi^{200}} \left[\frac{F_{S,100}}{F_{F,200}} \right]^2 \tag{7}$$

$I_{100 \text{ or } 200}$ = Intensity (counts under peak) of 100 or 200 from experimental data.
$\phi^{100 \text{ or } 200}$ = Lorentz and polarization correction factors.
$F_{S,100 \text{ or } F,200}$ = Equations (5) and (6)

The remaining unknown is V_f, the volume fraction of δ', which can now be solved for.

E. SCOPE OF PRESENT WORK

Although many TEM studies of the δ' precipitate have been completed, particle size determination by X-Ray diffraction (and the Scherrer equation) has *not* been conducted. Also the amount of size data available covering the as quenched to peak strength aging time span is minimal. The peak strength size (≈300Å) and spherical particle shape of δ' lends itself well to X-Ray analysis. It is for these reasons, and the other advantages of X-Ray diffraction over TEM (e.g., larger sampling size, lack of electopolishing losses, etc.), that this thesis was conducted.

From the X-Ray data obtained the following objectives intend to be accomplished:

- Validate the use of X-Ray methods in examining Al-Li alloys.
- Calculate δ' particle size in the as quenched condition and during a 32 hour age (@ 194°C). Verify with TEM results.
- Document the existence of δ' or ordered regions in the alloy in the quenched state.
- Calculate the volume fraction of δ' in the as quenched state.

III. EXPERIMENTAL

A. SAMPLE PREPARATION

Sample specimens were obtained from a hot rolled .056 in. thick sheet of aluminum alloy, designated P54, supplied by Alcan International Ltd. The compositional make-up was Al-2.5%Li-0.15%Zr, by weight (Al-9.073%Li-0.0414%Zr atomic). 1.0 by .75 in. samples were cut from the sheet. Sanding and polishing, down to a 1 micron diamond polish, was conducted prior to solution heat treating in order to allow the heat treatment to remove any material strain which would adversely affect the X-Ray diffraction results.

The solution heat treatment was conducted at 460°C for 35 minutes. Due to the reported [Ref.40] losses of lithium from high temperature oxidation, the samples were enclosed in an argon filled glass tube. The quenching medium was ice brine.

B. X-RAY DIFFRACTION

Preparation of the sample for the x-ray diffraction scan consisted of a six, three and one micron diamond polishing. Care was taken not to overstrain or overheat the sample due to excessive polishing pressure. A 30 second etch with Keller's reagent (1%HF/1.5%HCl/2.5%HNO_3/95% H_2O) concluded the preparation.

The x-ray equipment consisted of a Philips XRG 3100 X-ray Generator (copper target, $\lambda = 1.5405$Å) and a Norelco Data Control and Processor. A 30kv, 35ma power setting, and a scan rate of 4 minutes per degree was used for obtaining all data. All intensity and line broadening values were obtained manually by measuring directly from the paper trace outputs. The 100($2\theta = 21.95°$), 110($2\theta = 32.14°$), 200($2\theta = 44.74°$) and 220($2\theta = 65.13°$) peaks were examined during each analysis.

The heat treatment consisted of suspending the sample pieces in boiling ethylene glycol (194-195°C). Ethylene glycol was used due to its boiling temperature agreeing favorably with the manufacturer's recommendation of 190°C (for peak strength in 32 hours) and because it would also provide an oxygen/moisture free environment (thus preventing lithium loss). Amount of heat treatment varied from none (as quenched) to 32 hours for the δ' study. An additional two weeks was allowed for δ verification at $2\theta = 24.15°$. Room temperature water was used for quenching.

Placement of the samples into the holder was exactly duplicated each time in order to ensure that the X-Ray beam contacted the same area of the sample for each exposure. During trial X-Ray scans it was noted that intensity values varied with varying placement of the sample. This phenomenon was considered due to the texturing of the material.

C. TEM

Sample #2, after 32 hours of aging, was sectioned with a diamond saw. 3mm. diameter TEM discs were punched out of the sectioned pieces. Electropolishing was carried out using a solution of 3% perchloric acid, 35% butoxy ethanol, and 62% ethanol. The "Tenupol" method was used at a temperature of -40°C and a potential of 40V.

A JEOL 100CX TEM, operating at 120kV, was used to examine the sample. Dark field images were photographed with g=(100) and beam direction B=[100].

D. LIGHT MICROSCOPE

An as quenched sample was mechanically polished down to 1 micron diamond paste. Electropolishing was carried out using a solution of 20% nitric acid in methanol, at a potential of 20V and at a temperature of -27°C. Anodising was conducted using Barker's Reagent (46ml. HBF_4, 7g. boric acid, 970ml. H_2O) A potential of 20V for 1 minute was used.

IV. RESULTS AND DISCUSSION

A. OPTICAL MICROSCOPE

Figure 5 is a micrograph of the alloy in the as quenched condition. No information concerning the δ' precipitate can be discerned due to its small size. The rolling direction of the sample is readily apparent as well as many numerous non-metallic inclusions.

Figure 5. Optical Micrograph of As Quenched Alloy

B. PARTICLE SIZE

A paper trace plot of Sample #2, the 100 peak, after 15 minutes of heat treatment is shown in Appendix C. The as quenched 100 peaks were easily discernable in both samples thus identifying the existence of ordered (superlattice) regions. A background baseline and the profile line were manually drawn in. The profiles were expected to grow and narrow as the aging treatment proceeded. The increase in particle size would narrow the diffracted range of 2θ and thus concentrate the energy over a shorter 2θ span (i.e., increasing the counts per second). This was observed as seen in the computer overlay in Figure 6 of Sample #2.

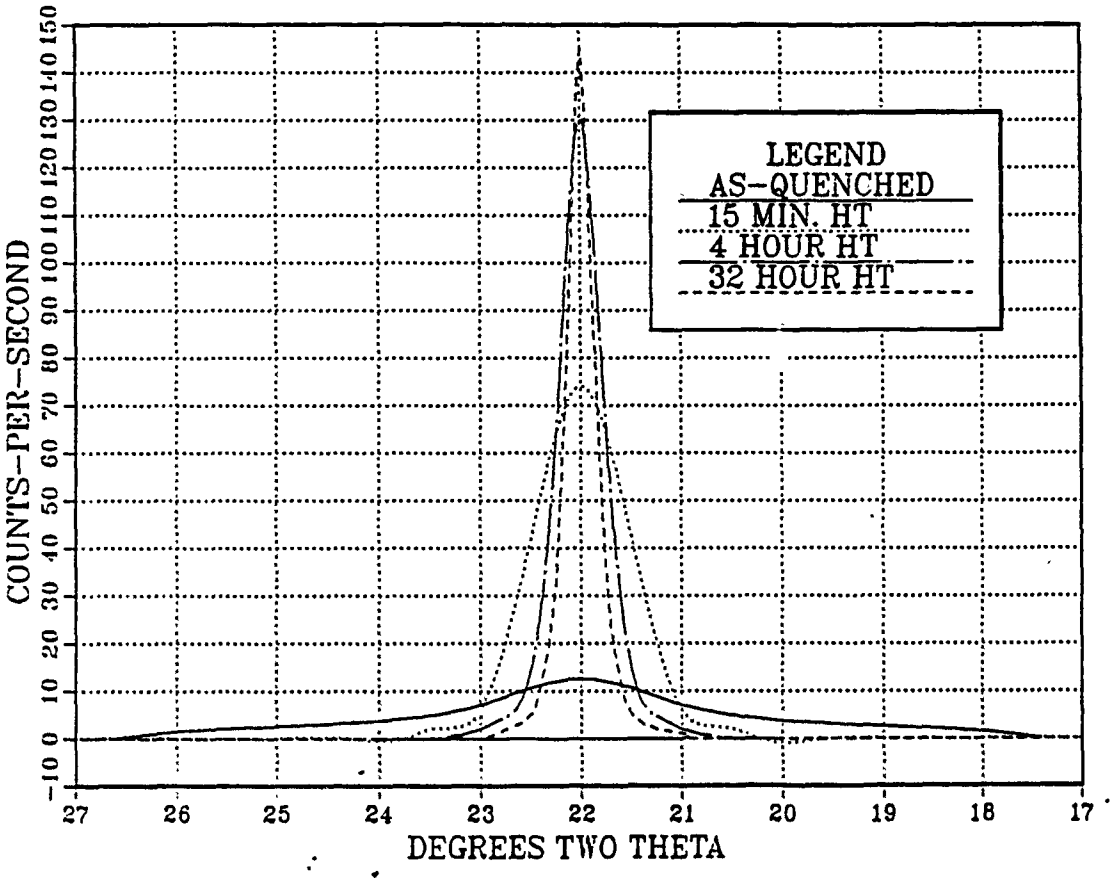

Figure 6. Sample #2 100 Peak Narrowing with Aging

In all X-Ray experiments with this alloy the 100 peak would rise first. The 110 peak was never seen in the as quenched samples. The 110 has been observed to begin rising after further heat treatment and to then surpass the 100 peak in intensity. (Although this was not observed in Samples #1 and #2.). The 100 peak for Sample #1, and the 110 peak for Sample #2, are shown in Appendices D and E. These observed intensities were extremely low. The scale is intentionally set as per the 100 peak of Sample #2 to demonstrate the texture of the alloy. The texture is the preferred orientation that is instilled in the material due to the rolling process. Error is easily introduced at this point in trying to curve fit such small curves against the background unless great care is taken.

The area ($in.^2$) underneath the profile was calculated using a planimeter. The following values were calculated from the paper trace outputs:

$$Intensity(counts) = \frac{1}{Chart\ speed(\frac{in.}{sec.})} \times \frac{No.\ of\ counts/sec.}{vert.\ scale\ in.} \times area(in.^2)$$

$$Integral\ Breadth(B,radians) = [Area(inches^2) \div height(inches)] \times \frac{.25°}{inch} \times .01745 \frac{radians}{1°}$$

Physical or strain broadening of these peaks was considered to be zero due to (1) the small ($<.2\%$) misfit strain of the δ' in the α matrix and (2) the sample material was hot rolled vice cold rolled. Instrumental broadening was determined by analyzing a sample of α quartz. The following values were obtained:

2θ	Instrumental Broadening (b,radians)
50.23	.003149
26.75	.002574
20.01	.002628

Interpolation values obtained for 21.9°(100 peak) and 31.2°(110) were .002613 and .002574 respectively. The pure profile, β, was then calculated using:

$$B^2 = b^2 + \beta^2$$

or

$$\beta = \sqrt{B^2 - b^2}$$

The particle size was calculated from:

$$L = \frac{K\lambda}{\beta \cos\theta}$$

Where $K = 1$, $\lambda = 1.5405$Å, θ equals half of 2θ, and β as just calculated. The intensity, integral breadth, instrumental broadening, actual broadening and particle radius are tabulated in Appendices A and B.

The particle size (radius) was plotted against aging time (hours) in Figure 7. Additional comparison TEM data points from Makin and Ralph [Ref.17] are included. Direct comparison data points are not available in the literature. Other research has either not tracked particle size at such early aging times, not used the same alloy percentage, or not used the same aging temperature. In general, though, the data obtained is in good agreement with other studies. Increased lithium, the presence of zirconium, and increased aging temperature will shift the graphs towards larger particle size. Makin and Ralph used a 3.08%wt.Li, .19%wt.Zr sample aged at 200°C versus the 2.5%wt.Li, .15%wt.Zr aged at 194°C used in this study. The comparison points are slightly higher, but this was expected due to their increased lithium content alloy.

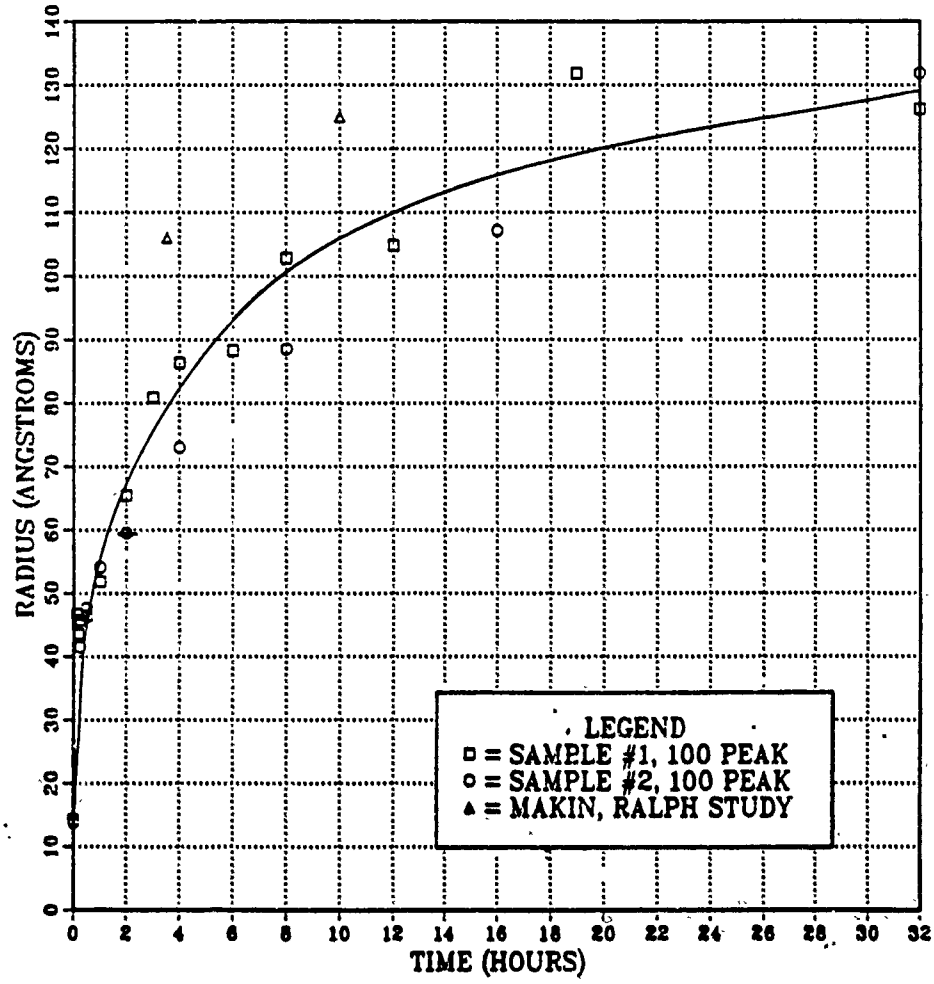

Figure 7. Particle Radius vs. Aging Time: Artificially aged at 194°C.

The as quenched particle diameter was found to be 28±3Å, and the 32 hour diameter 264±12Å (Sample #2, 100). A High Resolution Electron Microscope (HREM) micrograph of an as quenched Al-Li alloy, taken at the University of California at Berkley, is shown in Figure 8. Although the ordered area is marked 50Å, it is difficult to resolve the particle boundaries of such small sizes with electron microscopes. Other researchers, using TEM, have reported as quenched particle sizes in the 20-40Å range. The X-Ray diffraction average particle size determination may be more accurate due to the larger sampling volume and less subjective analysis of particle boundaries.

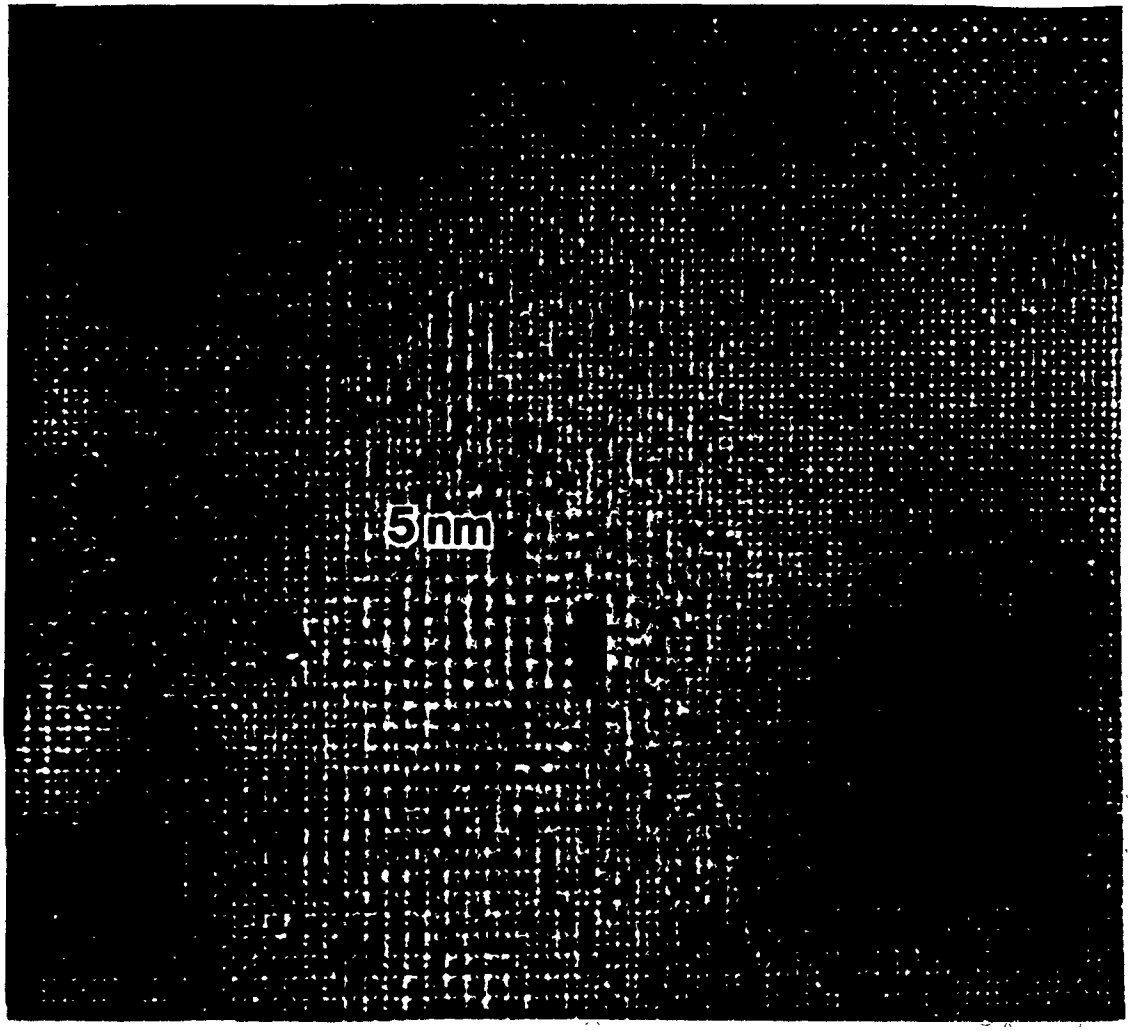

Figure 8. HREM Micrograph of an As Quenched Al-Li Alloy: Beam direction, B = [100]. A 50Å(5nm.) ordered area is marked. This is the developing δ' particle. (Micrograph courtesy A.G. Fox)

The alloy manufacturer recommended 32 hours @ 190°C for peak strength. δ' size at peak strength has been reported as ≈300-500Å. for all compositions/aging temperatures [Refs.34,19,35]. Thus, the experimental value of 264Å at first appears low. A TEM micrograph, after 32 hours aging, was taken of Sample #2 at NPS to measure particle size. Figure 9 shows an entire grain. δ' spheres are easily seen in the matrix. Al_3Zr surrounded by δ' shells are also easily identified (see arrow). A Precipitate Free Zone (PFZ) is also seen along the grain boundary.

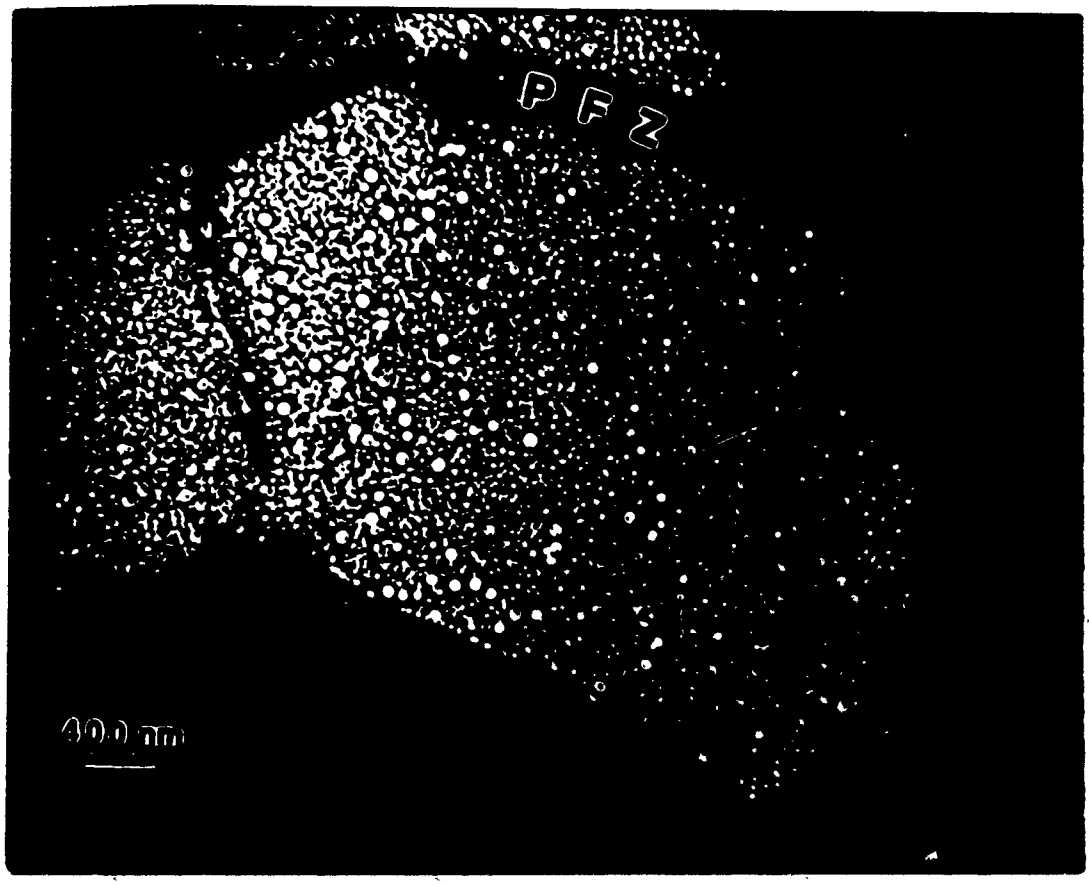

Figure 9. TEM Micrograph of Sample #2 at 32 Hour Age: Dark field image with g=(100) and B=[100]. δ' is easily seen. Also note shells of δ' surrounding Al_3Zr (arrow). Grain boundaries also contain precipitate free zones(PFZ).

A close-up of Figure 9 on page 26 is shown in Figure 10. One hundred particles were counted and measured. The average diameter was 269Å, with a standard deviation of 72 Å. The range was 113-752Å. These values are in excellent agreement with the X-Ray diffraction value of 264±12Å. Note that only the average value is seen by the diffraction measurements. Range values cannot be determined.

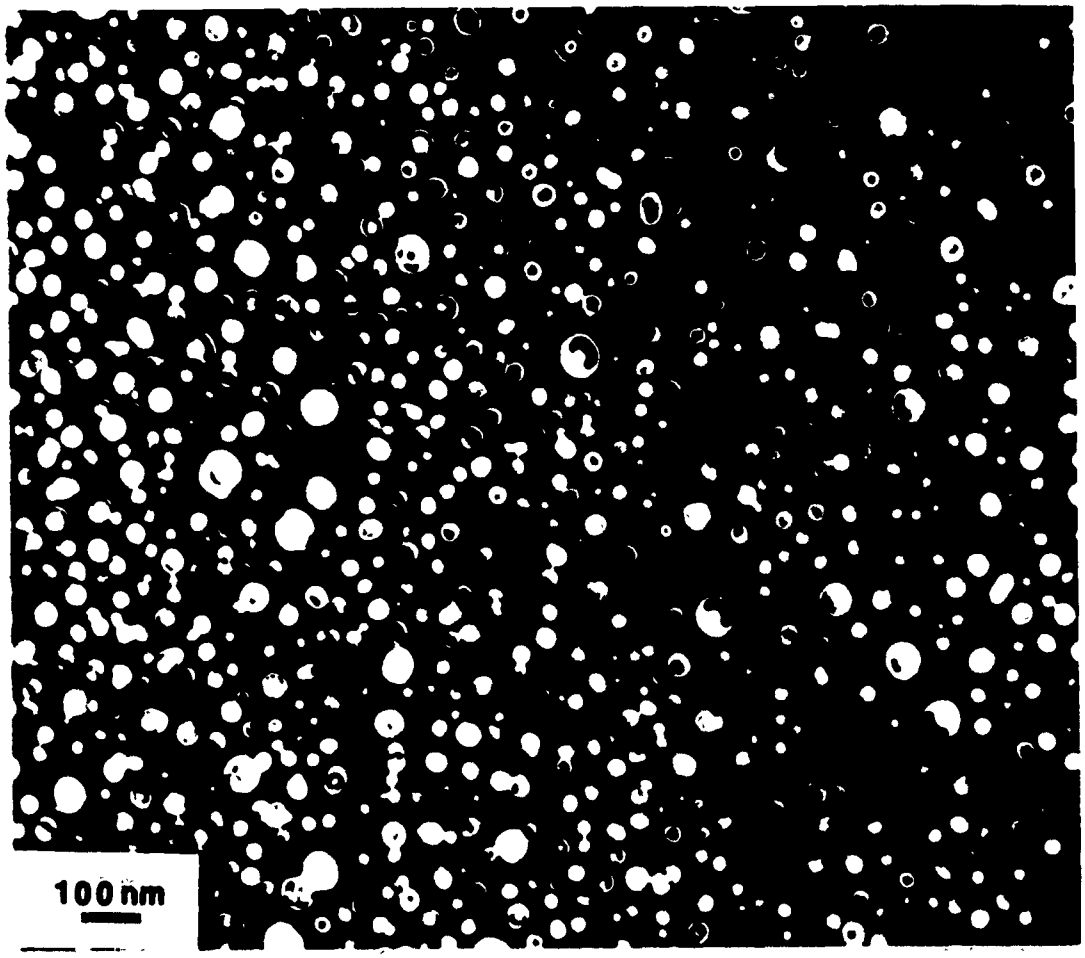

Figure 10. **TEM Micrograph of Sample #2 at 32 Hour Age (Close-up): Dark Field Image., B = [100]. Average diameter of δ' particles (includes *Al,Zr*) was 269Å.**

Particle radii were then cubed and plotted against time (Figure 11). A straight line can be drawn through the points. Note that only Sample #2, 100 peak points were used. Due to the large size, and thus easy measurability, of these peaks they were considered the most accurate. The scatter of the other points is assumed due to inaccuracies in profile area calculations.

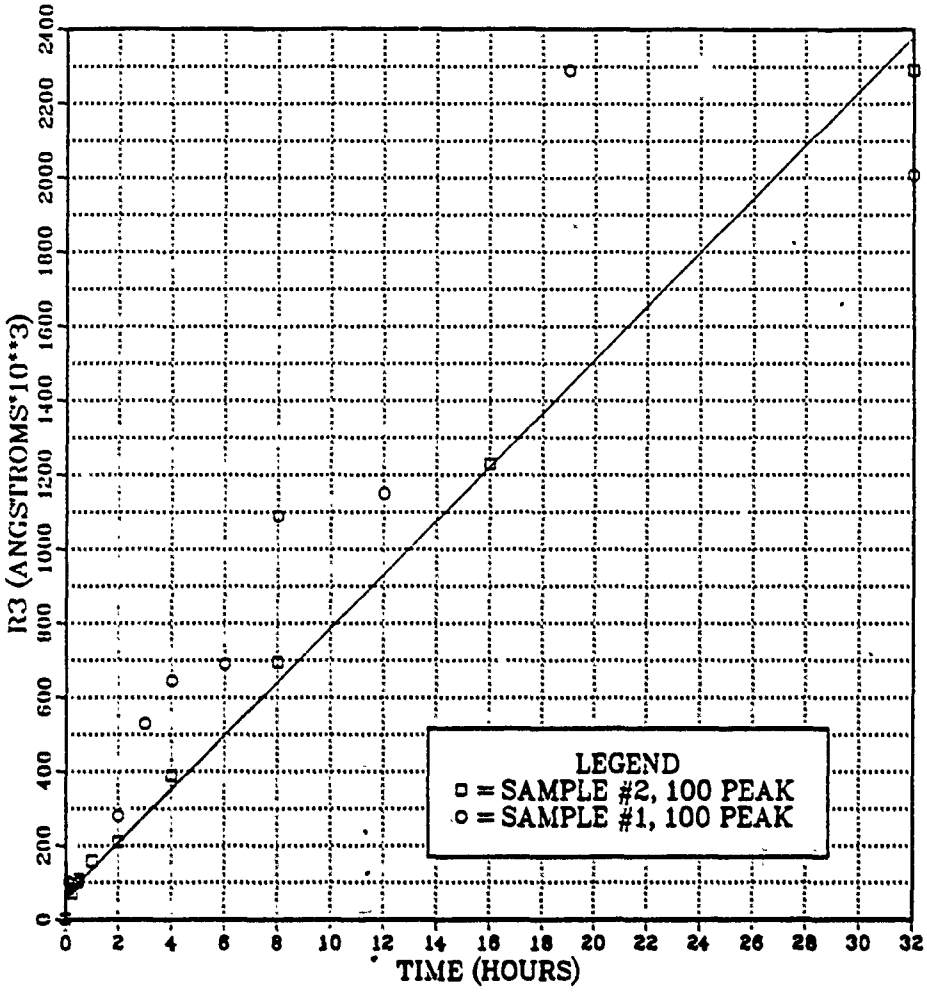

Figure 11. Particle Radius Cubed vs. Time (0 to 32 hours): Sample #2 particle size data (100 peak) was considered to be the most accurate (highest intensity) and the data from this was therefore used to generate the straight line shown in the diagram.

The straight line signifies that the growth is following Ostwald Ripening Kinetics (*radius*^{3} = *constant* × time). In normal nucleation and growth, the line should intersect zero. A close-up of the graph (Figure 12) indicates that the line does not intersect at zero. The effects of the order/disorder reaction or the spinodal decomposition may be altering the growth kinetics at, and shortly after, the quench.

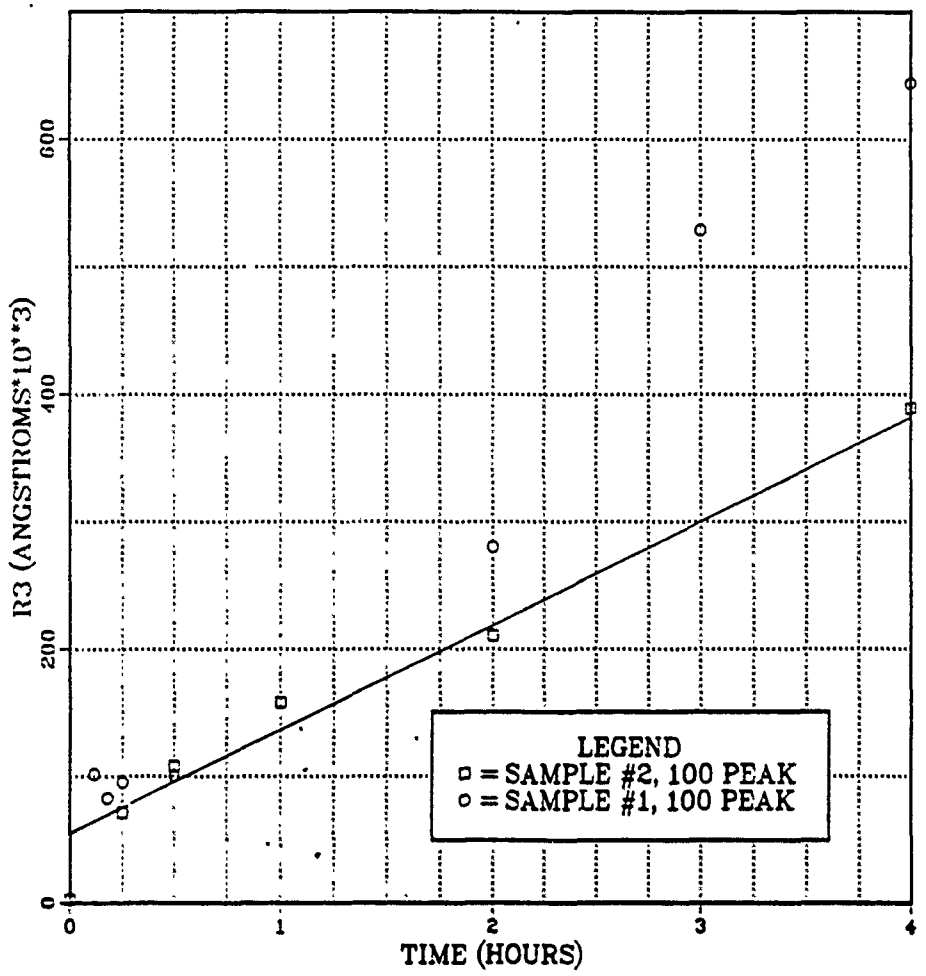

Figure 12. Particle Radius Cubed vs. Time (0 to 4 hours): The graph line does not track to zero. This may be due to the spinodal decomposition.

C. DELTA(AL-LI) FORMATION

The earliest indication of δ(Al-Li) formation in other research has occurred at .25 hours, using TEM [Ref.24]. A diffraction profile was observed in all samples (including practice runs previous to this study) in as quenched and at all aging times of this alloy at $2\theta \approx 24.14°$. This location corresponds to the 111 plane of the δ cubic ($a_o = 6.38$Å). The actual output trace of the δ peak can be seen in Appendix C. This same peak was also noted in previous samples (same composition) which were solution treated at 542°C (as compared to 460°C for #1 and #2). In Figure 13, the δ peaks are overlayed. A discernible intensity increase is seen with aging, but profile narrowing is not apparent.

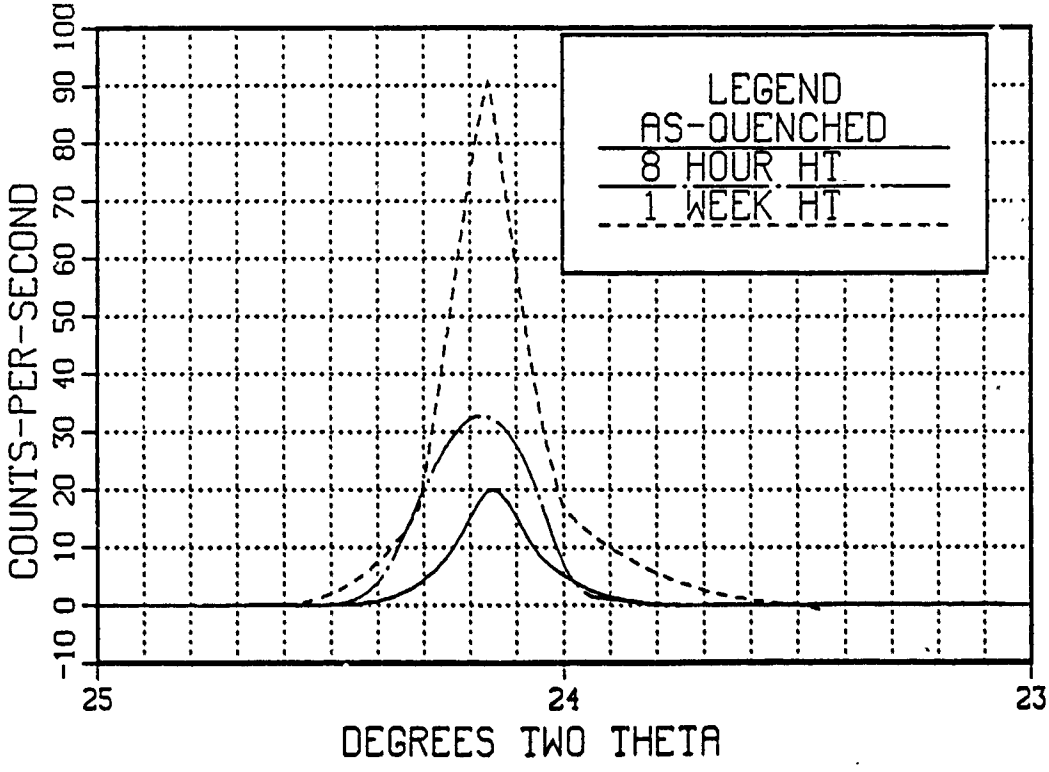

Figure 13. Delta(Al-Li) 111 Peak Growth (As quenched to Two Weeks): Peak narrowing is not apparent.

Intensity and particle size data is tabulated in Table 4. Although a general trend increase is seen, the data is sporadic. This could be due to the small amount of δ or to the non-spherical shape of the δ precipitate (reported as plate shaped,[Ref.41]). The presence of the δ in the as quenched condition is critical to the δ formation theories. Possibly, all initial (to peak age) δ growth may only be growth and not a δ' transformation as has been commonly thought [Refs.42,25]. Even recent (1988) δ' volume fraction studies (Williams, [Ref.43]) have assumed no δ formation. Any presence of δ, especially along grain boundaries, is considered detrimental to the fracture toughness of the alloy. The fact that δ always seems to be present even in as quenched Al-Li alloys is important new information which must be addressed when considering the properties of this alloy system.

Table 4. DELTA PHASE EXPERIMENTAL AND CALCULATED VALUES

Heat Treatment @194°C	Intensity (counts $\times 10^3$)	Pure Breadth (radians $\times 10^{-3}$)	Particle Size (Å)
As Quenched	1.02	3.232	487.3
30 min.	1.38	5.303	297.1
2 hours	1.62	3.125	504.0
3 hours	1.20	3.246	485.8
8 hours	2.10	4.381	359.6
19 hours	2.55	4.208	374.3
32hours	3.48	2.744	573.9
1 week	4.74	2.401	656.1
2 weeks	3.72	2.575	611.7

D. VOLUME FRACTION OF DELTA PRIME

The volume fraction of δ' in the as quenched condition was calculated as per the development in Background Section D.2.

Beginning with structure factor equations (3) and (4), the following values were used:

Subscripts B = Al and A = Li

Free atom form factors were calculated using the following summation:

$$f = \sum_{i=1}^{4} a_i \exp\left(-b_i\left(\sin^2\frac{\theta}{\lambda^2}\right)\right) + C$$

Where the values for a_i, b_i and C were obtained from [Ref.39].
For Al:

$$f^{200} = 8.50771 \qquad f^{100} = 10.6442$$

For Li:

$$f^{200} = 1.63140 \qquad f^{100} = 2.0422$$

Atomic fractions, disregarding zirconium content, will consist of two extremes:

(a)If α(matrix) and δ' are ordered and of the same composition:

$$m_{Li}^{\alpha} = .091 \quad m_{Al}^{\alpha} = .909 \quad m_{Li}^{\delta'} = .091 \quad m_{Al}^{\delta'} = .909$$

(b)If α(matrix) and δ' are ordered and the composition of the miscibility gap has been reached:

$$m_{Li}^{\alpha} = .055 \quad m_{Al}^{\alpha} = .945 \quad m_{Li}^{\delta'} = .25 \quad m_{Al}^{\delta'} = .75$$

Lorentz and polarization correction ratios are [Ref.38,p.894]:

$$\frac{\phi^{100}}{\phi^{200}} = \frac{53.7003}{11.5220} = 4.66067$$

The intensity ratio from experimental data is:

$$\frac{I_{100}}{I_{200}} = \frac{10.2 \times 10^3}{877.5 \times 10^3} = .01162$$

Solving for V_f in equation (7), the volume fraction for situation (a), same composition, is 25.3%, and for (b), miscibility gap compositions, is 29.3%. The actual compositions of α and δ' are probably in between the two extremes. Thus, the actual volume fraction is in the range of 25.3-29.3%. The range of the volume fraction is less than the values obtained by Williams [Ref.43], e.g. 37% after aging at 155°C, but this is almost certainly due to the difference in alloy compositions (12.7% vs. 9.% this study).

E. ERROR ANALYSIS

The major error source is considered the diffraction profile measurement. Pure profile breadth error is directly proportional to particle size error. The following error analysis was used:

$$\frac{d\beta}{\beta} = \frac{\sqrt{N_e}}{N_e} + \frac{dh_e}{h_e} + \frac{\sqrt{N_s}}{N_s} + \frac{dh_s}{h_s}$$

β = Pure profile breadth

N_e = No. of counts under experimental peak

h_e = Height of experimental peak

N_s = No. of counts under quartz standard peak

h_s = Height of quartz standard peak

dh = .1in. (accuracy of measurement)

Derivation of $\frac{\sqrt{N}}{N}$ is explained in pp. 361-364 of Ref. 38. The convergence of five planimeter readings was used. Planimeter and background errors are not included in this analysis. Error values for various heat treatment times are listed in Table 5.

Table 5. ERROR ANALYSIS VALUES

Heat Treatment Time (hours)	Error (%) $\frac{d\beta}{\beta}$
0	11.0
.5	5.20
2	4.88
8	5.96
16	4.49
32	4.60

V. SUMMARY

All previous studies of Al-Li alloys have used TEM to monitor δ' average particle size. The use of X-Ray diffraction techniques and the Scherrer equation were used successfully in this study to to track the δ' particle growth in a Al-2.5%Li-.15%Zr(wt.) alloy during aging at 194°C. Verification of the technique was accomplished by examining a sample at the end of the 32 hour heat treatment with the NPS TEM. X-Ray results produced an average diameter of 264±12Å. TEM particle counting gave a value of 269Å. Thus, the method can be considered valid. Due to the use of plate material for analysis though, discretion must be used in choosing the largest diffraction profiles for analysis. Texturing of the material causes large fluctuations in intensity values from sample to sample.

Superlattice peaks were observed in the as quenched sample. These greatly broadened (over eight degrees) profiles indicate the presence of very small ordered regions or δ' particles. This evidence supports the current order/disorder and spinodal decomposition theories.

The volume fraction of δ' in the as quenched sample assuming only ordering and no decomposition was 25.3%; assuming complete decomposition was 29.3%. The actual volume fraction is within this 25.3-29.3% range. This value agrees with other reported volume fractions after corrections for composition differences.

A diffraction profile was identified at $2\theta = 24.14°$ as the 111 reflection of the δ cubic intermetallic phase. This peak was observed during the entire heat treatment, including the as quenched. No other reports, in the literature, could be found of δ being present at such an early aging time. This finding may have important implications for microstructural development, and thus mechanical properties, in Al-Li alloys not previously considered.

VI. CONCLUSIONS

The following conclusions are drawn from this study:

- X-Ray diffraction analysis is effective in determining precipitate size (up to 270Å) for this Al-Li alloy.
- When applying this analysis to rolled materials of this type alloy, accuracy is greatly dependent upon the texture encountered in the sample piece. X-Ray diffraction profiles, for the same crystal plane, can vary immensely from sample to sample. The specific profile being analyzed must sufficiently stand out from the background noise to facilitate ease of measuring.
- X-Ray superlattice peaks were observed in the as quenched alloy. This is evidence of immediately formed δ' or ordered regions, thus supporting an order/disorder and spinodal decomposition theory.
- δ' volume fraction in the as quenched condition for this alloy is 25.3-29.3%.
- A δ(Al-Li) X-Ray diffraction peak was observed even in the as quenched alloy. This peak continued to grow during the 32 hour age.

VII. RECOMMENDATIONS

For further research, the following recommendations are given:

- Although this X-Ray method has been shown to effectively gage the δ' particle size, only one diffraction peak of sufficient size (and thus accuracy) was confidently examined. This analysis should be repeated with another similar peak from another sample to insure reproducibility.

- This analysis program needs to be extended to alloys of other lithium contents, and also to commercial alloys such as 2090, in order to try and completely understand the aging process in Al-Li alloys.

- The detection of the δ phase in the as quenched sample by this analysis is a major step in understanding the microstructural development of Al-Li alloys. Due to the detrimental nature (low toughness) of this phase, additional research to check the development of δ in other Al-Li alloy systems is warranted.

APPENDIX A. EXPERIMENTAL DATA FOR SAMPLE #1

Table 6. EXPERIMENTAL DATA FOR SAMPLE #1, (0 TO 2 HOURS)

Heat Treatment	Peak	Intensity (counts $\times 10^3$)	Integral Breadth (radians $\times 10^{-3}$)	Instrumental Broadening (radians $\times 10^{-3}$)	Actual Broadening (radians $\times 10^{-3}$)	Particle Radius Å
As Quenched	100	2.28	55.27-	2.613	55.20	14.21
	110	--.--	--.---	2.574	--.--	--.--
	200	174.--	3.397			
	220	30.0-	4.545			
1 Minute	100	--.--	--.--	2.613	--.--	--.--
	110	--.--	--.--	2.574	--.--	--.--
	200	--.--	--.--			
	220	--.--	--.--			
7 Minutes	100	2.34	17.02-	2.613	16.82	46.65
	110	.72	(?)17.45-	2.574	17.26	46.38
	200	120.--	3.293			
	220	27.0-	4.007			
11 Minutes	100	2.88	18.21-	2.613	18.02	43.54
	110	--.--	--.---	2.574	--.--	--.--
	200	138.--	3.206			
	220	28.2-	4.429			
15 Minutes	100	2.94	17.38-	2.613	17.18	45.66
	110	--.78	17.19-	2.574	16.00	49.99
	200	129.--	3.153			
	220	28.2-	3.998			
30 Minutes	100	2.94	17.10-	2.613	16.89	46.45
	110	--.--	--.---	2.574	--.--	--.--
	200	123.--	3.253			
	220	31.2-	4.088			
1 Hour	100	2.64	15.36-	2.613	15.14	51.82
	110	-.84	16.08-	2.574	15.87	50.40
	200	123.--	3.440			
	220	33.6-	3.941			
2 Hours	100	2.70	12.27-	2.613	11.99	65.44
	110	1.20	17.45-	2.574	17.26	46.33
	200	96.0-	3.103			
	220	36.0-	4.059			

Table 7. EXPERIMENTAL DATA FOR SAMPLE #1, (3 TO 32 HOURS)

Heat Treatment	Peak	Intensity (counts × 10^3)	Integral Breadth (radians × 10^{-3})	Instrumental Broadening (radians × 10^{-3})	Actual Broadening (radians × 10^{-3})	Particle Radius Å
3 Hours	100	2.28	10.05-	2.613	9.704	80.85
	110	--.90	13.09-	2.574	12.83-	62.34
	200	105.--	3.394			
	220	37.2-	4.227			
4 Hours	100	2.34	9.454	2.613	9.086	86.35
	110	-.90	11.29-	2.574	10.99-	72.75
	200	109.--	3.342			
	220	37.8-	4.433			
6 Hours	100	3.12	9.261	2.613	8.885	88.31
	110	1.08	10.47-	2.574	10.15-	78.79
	200	120.--	3.293			
	220	42.0-	4.156			
8 Hours	100	2.76	8.063-	2.613	7.628	102.8
	110	1.20	10.91-	2.574	10.60-	75.45
	200	105.--	3.393			
	220	37.8-	4.433			
12 Hours	100	2.40	7.933	2.613	7.490	104.8
	110	-.84	7.636	2.574	7.189	111.25
	200	102.--	3.451			
	220	40.2-	4.280			
19 Hours	100	2.28	6.501	2.613	5.953	131.8
	110	1.20	8.311	2.574	7.902	101.2
	200	96.0-	3.348			
	220	40.8-	4.428			
32 Hours	100	1.92	6.746	2.613	6.219	126.16
	110	1.08	6.042	2.574	5.466	146.32
	200	78.0-	3.412			
	220	54.0-	4.178			

APPENDIX B. EXPERIMENTAL DATA FOR SAMPLE #2

Table 8. EXPERIMENTAL DATA FOR SAMPLE #2, (0 TO 32 HOURS)

Heat Treatment	Peak	Intensity (counts × 10^3)	Integral Breadth (radians × 10^{-3})	Instrumental Broadening (radians × 10^{-3})	Actual Broadening (radians × 10^{-3})	Particle Radius Å
As Quenched	100	10.2-	57.06-	2.613	57.00	13.76
	110	--.--	--.---	2.574	--.--	--.--
	200	878.--	3.191			
	220	12.1-	6.481			
15 Minutes	100	19.4-	19.10	2.613	18.92	41.47
	110	--.--	--.--	2.574	--.--	--.--
	200	810.--	2.756			
	220	10.32	5.003			
30 Minutes	100	21.12	16.69-	2.613	16.48	47.61
	110	--.--	--.---	2.574	--.--	--.--
	200	825.3-	2.727			
	220	9.12	5.024			
1 Hour	100	20.28	14.75-	2.613	14.52	54.04
	110	--.--	--.---	2.574	--.--	--.--
	200	780.--	2.793			
	220	8.52	4.363			
2 Hour	100	20.16	13.45-	2.613	13.19	59.48
	110	--.--	--.---	2.574	--.--	--.--
	200	720.--	2.846			
	220	13.9-	4.459			
4 Hours	100	19.9-	11.06-	2.613	10.75	72.98
	110	--.--	--.---	2.574	--.--	--.--
	200	732.--	2.877			
	220	14.4-	4.957			
8 Hours	100	21.6-	9.240	2.613	8.863	88.54
	110	-.60	10.91-	2.574	8.531	93.75
	200	708.--	3.029			
	220	22.5-	4.142			
16 Hours	100	15.7	7.777	2.613	7.325	107.1
	110	.84	8.727	2.574	8.339	95.91
	200	552.--	3.088			
	220	30.--	3.636			
32 Hours	100	12.96	6.500	2.613	5.952	131.8
	110	.90	8.727	2.574	8.339	95.91
	200	492.--	2.909			
	220	36.0-	3.794			

APPENDIX C. ACTUAL EXPERIMENTAL OUTPUT

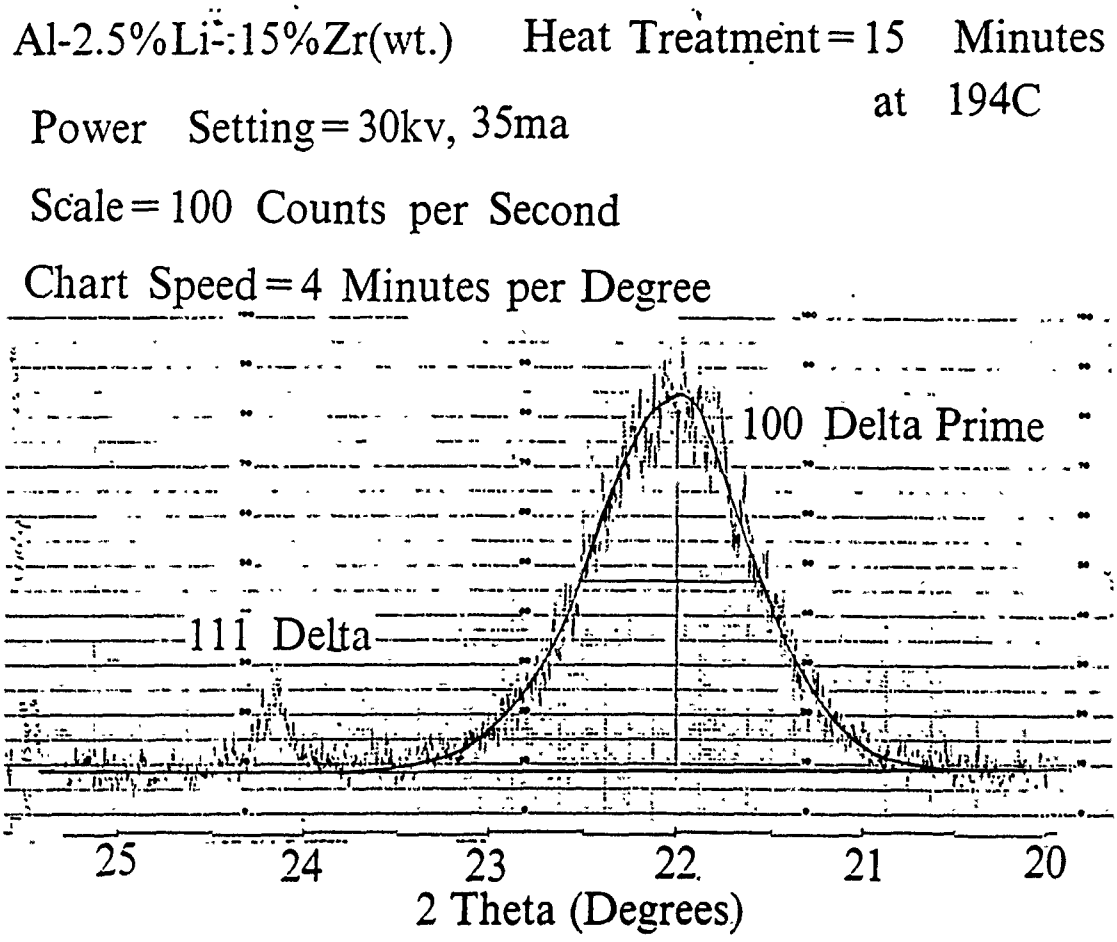

Figure 14. Sample #2, 100 Peak, Actual Experimental Output: 15 minute heat treatment. The 100 peak is easily measured. The δ 111 peak is clearly present. Background and curve lines manually drawn.

APPENDIX D. SAMPLE #1, 100 PEAKS

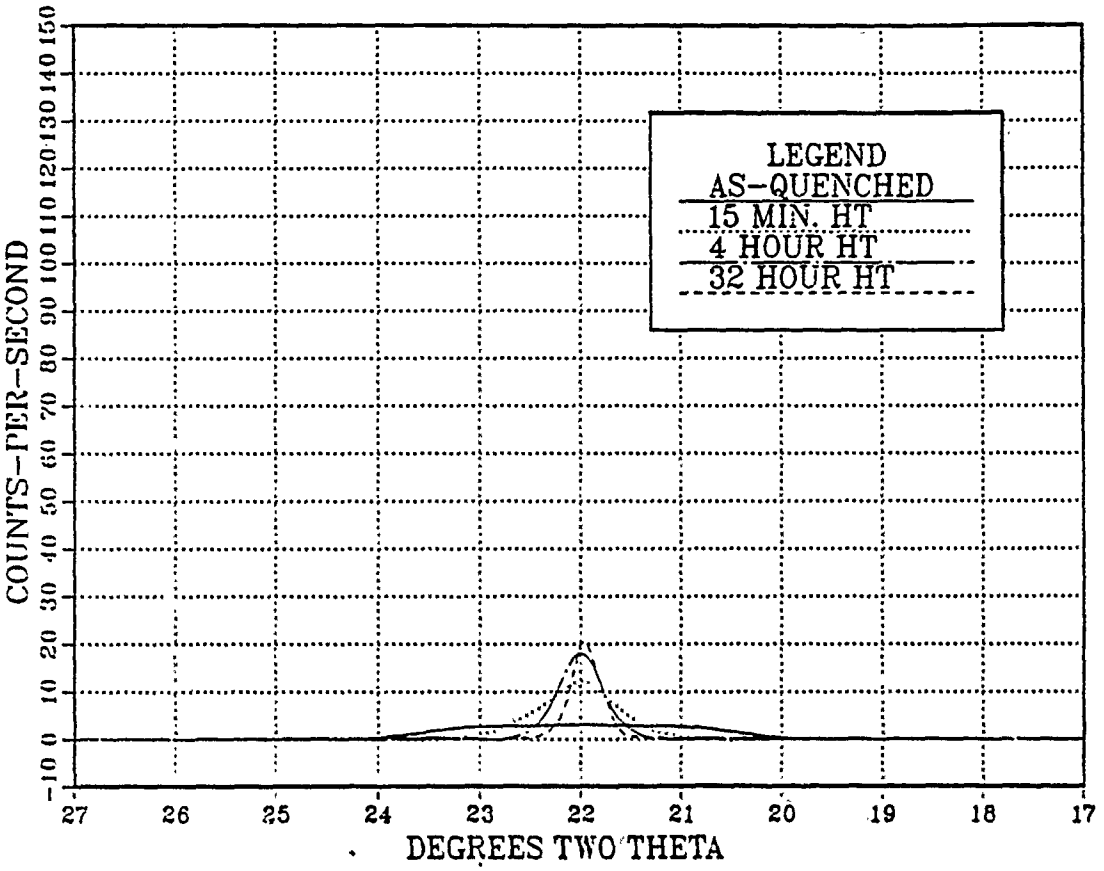

Figure 15. Sample #1 100 Peak Growth Overlay: This graph was intentionally left at the same scale as the 100 peak from Sample #2 to illustrate the variance in results from sample to sample. All samples were cut from the same rolled sheet in close proximity. It is assumed that this difference is due to the texture of the material, i.e. preferential directions have been attained by the crystal structures due to the rolling.

APPENDIX E. SAMPLE #2, 110 PEAKS

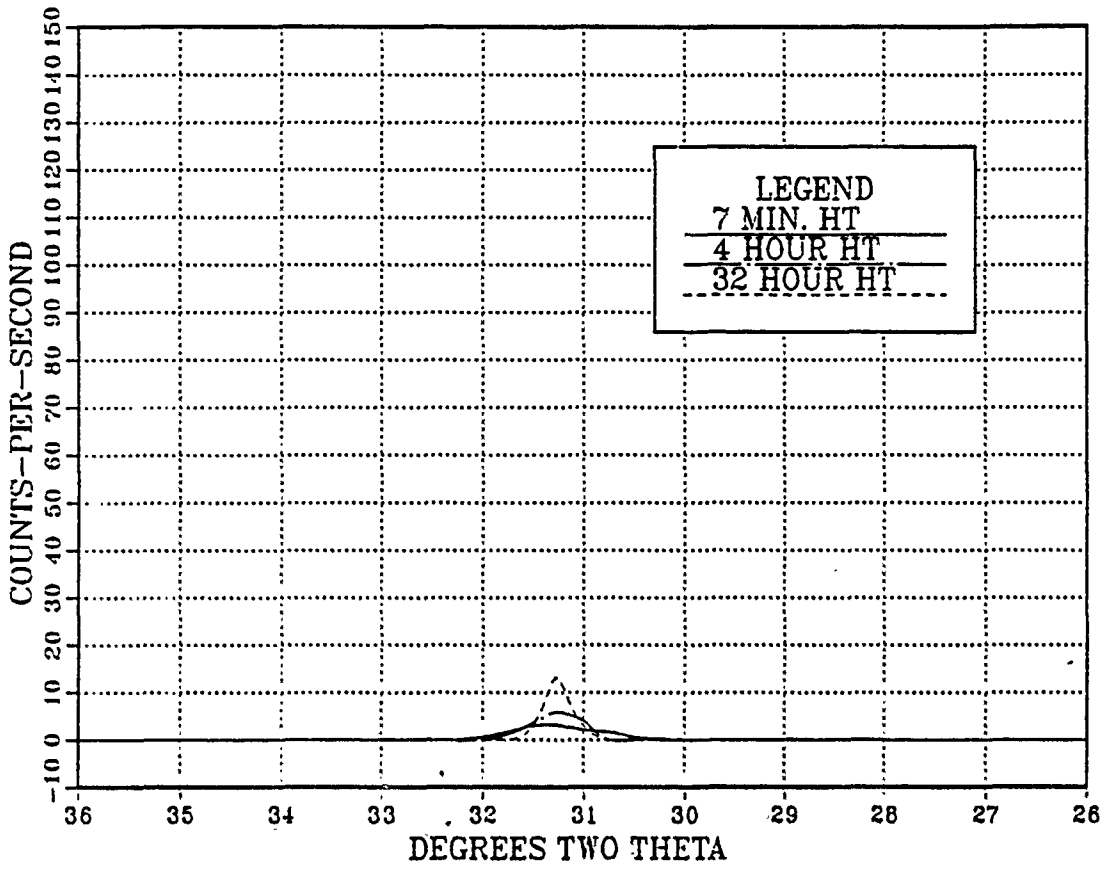

Figure 16. Sample #1 110 Peak Growth Overlay: This graph was intentionally left at the same scale as the other graphs for direct intensity comparison. The 110 peak was never seen in the as quenched condition. The low intensity of these peaks will result in greater inaccuracies in the particle size determination. In other trial runs prior to this particular study, the 110 peak has displayed dramatic growth during the the aging process.

LIST OF REFERENCES

1. Balmuth, E. S., and Schmidt, R., "A Perspective on the Development of Aluminum-Lithium Alloys", *Aluminum-Lithium Alloys*, Sanders, T. H. and Starke, E. A., eds., The Metallurgical Society of AIME, 1981.

2. Prichett, T. R., "Advanced Technology Aluminum Materials for Aerospace Applications", *Aluminum Technology'86*, Sheppard, T., ed., Institute of Metals, 1986.

3. Peel, C. J., and others, "The Development and Application of Improved Al-Li Alloys" *Aluminum-Lithium Alloys II*, Sanders, T. H. and Starke, E. A., eds., The Metallurgical Society of AIME, 1984.

4. Little, D., "Overview", *Al-Li Alloys III, University of Oxford, 8-11 July 1985*, Gregson, P.J., Harrison, S.J., and Peel, C.J.,eds.,Institute of Metals, London, 1986.

5. Wadsworth, J. "Superplasticity Behavior of Al-Li Alloys", *Aluminum-Lithium Alloys II*, Sanders, T. H. and Starke, E. A., eds., The Metallurgical Society of AIME, 1984.

6. Phonecon with J. Kozol of Naval Air Development Center, Warminster, PA., February 26, 1990.

7. Roy, G., "Status of Al-Li Development at Pechiney", *l-Li Conference, March 25-26, 1987, Los Angeles, Ca.*, Ramesh, J.,Suphal, P., and Quist, W. eds., ASM 1987.

8. Evans, R. K., "Western World Lithium Reserves" *Al-Li Alloys III, University of Oxford, 8-11 July 1985*, Gregson, P.J., Harrison, S.J., and Peel, C.J.,eds.,Institute of Metals, London, 1986.

9. Forness, S. and Heckman, E. A. W., "The Use of 8090 in the McDonell-Douglas F15 SMTD Aircraft", *Al-Li Conference, March 25-26, 1987, Los Angeles, Ca.*, Ramesh, J.,Suphal, P., and Quist, W. eds., ASM 1987.

10. Waldman, J.,Mahapatra, R., Neu, C., "Al-Li Alloys for Navy Aircraft", *Al-Li Conference, March 25-26, 1987, Los Angeles, Ca.*, Ramesh, J.,Suphal, P., and Quist, W. eds., ASM 1987.

11. Sung,C. M., Chan, H. M., and Williams, D. B., "Quantitative Microanalysis of Li in binary Al-Li Alloys", *Al-Li Alloys III, University of Oxford, 8-11 July 1985*, Gregson, P.J., Harrison, S.J., and Peel, C.J.,eds.,Institute of Metals, London, 1986.

12. Chan, H. M., Williams, D.B., "Quantitative Analysis of Lithium in Al-Li Alloys by Ionization Energy Loss Spectroscopy", *Phil. Mag.*, Vol.52, No.5, 1019-1032, 1985.

13. Pickering, H. W., "(1) Atomistic Study of Metastable Phases in an Al-3wt.%Li-0.12%-Zr Alloy ,(2)A Preliminary Study of Al-Li Alloys using Atom-Probe Field Ion Micros copy and Transmission Electron Microscopy", *Office of Naval Research Technical Report No. N00014-84-k-0201, 2 March 1987.*

14. Spooner, S., Williams, D., Sung, C., "Combined Small Angle X-Ray Scattering and Transmission Electron Microscopy Studies of Al-Li Alloys", *Al-Li Alloys III, University of Oxford, 8-11 July 1985*, Gregson, P.J., Harrison, S.J., and Peel, C.J.,eds.,Institute of Metals, London, 1986.

15. Sigli, C. and Sanchez, J. M., "Calculation of Phase Equilibrium in Al-Li Alloys", *Acta. Metall.*, Vol.34, No.6, pp. 1021-1028, 1986.

16. Mahalingam, K., Gu, B. P., Liedl, G. L., and Sanders, T. H., "Coarsening of δ'(A l_3 Li) Precipitates in Binary Al-Li Alloys", *Acta. Metall.* Vol. 35, No. 2, pp. 483-498, 1987.

17. Makin, P. L. and Ralph, B., "On the Ageing of an Aluminum-Lithium-Zirconium Alloy", *J. Mat. Sci.*, 19, pp.3835-3843, 1984.

18. Cocco, G.,Fagherazzi, G. and Schiffini, L., "Determination of the δ' Coherent Miscibility Gap in the Al-Li System by Small-Angle X-Ray Scattering", *J. Appl. Cryst.*, Vol.10, pp.325-327, 1977.

19. Gu, B., Mahalingam, K., Liedl,G. L., and Sanders, T. H., "The Delta Prime Particle Size Distributions in a Variety of Al-Li Alloys" *Al-Li Alloys III, University of Oxford, 8-11 July 1985*, Gregson, P.J., Harrison, S.J., and Peel, C.J.,eds.,Institute of Metals, London, 1986.

20. Gu, B. P., Liedl, G.L., Kulwicki, J. H., Sanders, T. H., "Coarsening of Delta Prime Precipitates in an Al-2.8Li-0.3Mn Alloy", *Mat. Sci. Eng.*, Vol. 70, pp. 217-228, 1985.

21. Vecchio, K. S. and Williams, D. B., "Convergent Beam Electron Diffraction Study of Al_3Zr and Al-Li-ZR Alloys", *Acta. Metall.* , Vol. 35, No. 12, pp.2959-2970, 1987.

22. Gregson, P. J. and Flower, H. M., "δ' Precipitation in Al-Li-Mg-Cu-Zr Alloys", *J. Mat. Sci. Letters*, 3, pp.829-834, 1984.

23. Williams, D. B., "Microstructural Characteristics of Al-Li Alloys" *Aluminum-Lithium Alloys*, Sanders, T. H. and Starke, E. A., eds., The Metallurgical Society of AIME, 1981.

24. Jha, S. C., Sanders, T. H., and Dayananda, M. A., "Grain Boundary Precipitate Free Zones in Al-Li Alloys", *Acta. Metall.*, Vol. 35, No. 2, pp. 473-482, 1987.

25. Quist, W. E., Narayanan, G. H., and Wingert, A. L., "Al-Li Alloys for Aircraft Structure-An Overview", *Aluminum-Lithium Alloys II*, Sanders, T. H. and Starke, E. A., eds., The Metallurgical Society of AIME, 1984.

26. Sanders, T. H. and Starke, E. A., "Overview of the Physical Metallurgy in the Al-Li-X System", *Aluminum-Lithium Alloys II*, Sanders, T. H. and Starke, E. A., eds., The Metallurgical Society of AIME, 1984.

27. Radmilovic, V., Fox, A. G. and Thomas, G., "Spinodal Decomposition of Al-Rich Al-Li Alloys", *Acta. Metall.*, Submitted 13 February, 1989.

28. Williams, D. B., and Edington, J. W., "The Precipitation of $\delta'(Al_3Li)$ in Dilute Aluminum-Lithium Alloys", *Metal Science*, Vol.9, pp.529-532, 1975.

29. Khachaturyan, A. G., Lindsey, T. F., and Morris, J. W., "Theoretical Investigation of the Precipitation of δ' in Al-Li", *Met. Trans. A*, Vol. 19A, Feb. 1988.

30. Sato, T., Tanaka, N., and Takahashi, T., "High Resolution Lattice Images of Ordered Structures in Al-Li Alloys", *Trans. JIM*, Vol. 29, No. 1, pp. 17-25, 1988.

31. Fox, A. G. and Fisher, R. M., "The Origin of the High Elastic Modulus in Al-Li Alloys", *J. Mat. Sci. Letters*, 7, pp. 301-303, 1988.

32. Fox, A. G. and Fisher, R. M., "Structure Factors and Debye Temperatures of Al-Li Solid-Solution Alloys", *Acta. Cryst.*, A43, pp.260-265, 1987.

33. Furukawa, M., Miura, Y., and Nemoto, M., "Strengthening Mechanisms in Al-Li Alloys Containing Coherent Ordered Particles", *Trans. JIM*, Vol.26, No.4, pp. 230-235, 1985.

34. Glazer, J., Edgecumbe, T. S., and Morris, J. W., "Theoretical Analysis of Aging Response of Al-Li Alloys Strengthened by Al_3Li Precipitates", *Al-Li Alloys III, University of Oxford, 8-11 July 1985*, Gregson, P.J., Harrison, S.J., and Peel, C.J.,eds.,Institute of Metals, London, 1986.

35. Furukawa, M., Miura, Y., and Nemoto, M., "Arrangement of Deformation Induced Dislocations in Aged Al-Li Alloys", *Trans. JIM*, Vol.26, No. 4, pp. 225-229,1985.

36. Noble, B., Harris, S.J., Dinsdale, K., "Yield Characteristics of Aluminum-Lithium Alloys" *Met. Sci.* Vol.16, No.9, Sept. 1982.

37. Sanders, T. H. and Starke, E. A., "The Effects of Slip Distribution on the Monotonic and Cyclic Ductility of Al-Li Binary Alloys", *Acta. Metall.*, Vol.30, pp.927-939, 1982.

38. Klug, H. P. and Alexander, L. E., *X-Ray Diffraction Procedures*, Chapter 9, John Wiley and Sons, 1974.

39. Warren, B. E., *X-Ray Diffraction*, Addison-Wesley, 1969.

40. Burke, M., Papazian, J. M., "Elevated Temperature Oxidation of Al-Li Alloys", *Al-Li Alloys III, University of Oxford, 8-11 July 1985*, Gregson, P.J., Harrison, S.J., and Peel, C.J.,eds.,Institute of Metals, London, 1986.

41. Noble, B. and Thompson, G. E., "Precipitation Characteristics of Aluminum-Lithium Alloys", *Met. Sci. J.*, Vol. 5, pp.114-120, 1971.

42. Sanders, T. H., "δ'(Al_3Li) Morphology and its Influence on the Mechanical Behavior of Aluminum-Lithium Alloys", *International Light Metals Conference, 8th*,1987.

43. Liu, D. R. and Williams, D. B., "Determination of the δ' Solvus Line in Al-Li Alloys by Measurement of the δ' Volume Fraction", *Scripta Metall.*, Vol. 22, pp. 1361-1365, 1988.

INITIAL DISTRIBUTION LIST

		No. Copies
1.	Defense Technical Information Center Cameron Station Alexandria, VA 22304-6145	2
2.	Library, Code 0142 Naval Postgraduate School Monterey, CA 93943-5002	2
3.	Naval Engineering Curricular Office, Code 34 Department of Mechanical Engineering Naval Postgraduate School Monterey, CA 93943-5100	1
4.	Prof. A. J. Healey, Code ME/HY Chairman Department of Mechanical Engineering Naval Postgraduate School Monterey, CA 93943-5100	1
5.	Prof. A.G. Fox, Code ME/FX Department of Mechanical Engineering Naval Postgraduate School Monterey, CA 93943-5100	3
6.	Prof. Terry R. McNelley, Code ME/MC Department of Mechanical Engineering Naval Postgraduate School Monterey, CA 93943-5100	1
7.	Dr. D.J. Michel, Code 6000 Naval Research Laboratory Washington, DC 22375	1
8.	Dr. George Yoder, Code 11 Office of Naval Research Balston Towers Arlington, VA	1
9.	Lt. C.E. Whitman, USN 177 (#3) OceanView Blvd. Pacific Grove, CA 93950	1
10.	Lt. E.F. Goodson, Sr. SWOSCOLCOM-DH CSE 112 Newport, RI 93943-5100	1

11. Capt. Wang Te-Kang (Taiwan Army) 1
SMC #1904
Naval Postgraduate School
Monterey, CA 93943-5100

12. Capt. Scott Fuller, USMC 1
SMC #1925
Naval Postgraduate School
Monterey, CA 93943-5100